Basin Research

IAS EAGE

Basin Research (2012) **24**, 1–22, doi: 10.1111/j.1365-2117.2011.00539.x

The evolution of the high-elevated depocenters of the northern Sierras Pampeanas (*ca.* 28° SL), Argentine broken foreland, South-Central Andes: the Pipanaco Basin

Federico M. Dávila,*,[1] Mario E. Giménez,† Julieta C. Nóbile* and M. Patricia Martínez†

*Centro de Análisis de Cuencas, CICTERRA-UNC, FCEFyN, Ciudad Universitaria, Córdoba, Argentina

†Instituto Geofísico-Sismológico Volponi, FCEFyN-UNSJ, San Juan, Argentina

ABSTRACT

The Pipanaco Basin, in the southern margin of the Andean Puna plateau at *ca.* 28°SL, is one of the largest and highest intermontane basins within the northernmost Argentine broken foreland. With a surface elevation >1000 m above sea level, this basin represents a strategic location to understand the subsidence and subsequent uplift history of high-elevation depositional surfaces within the distal Andean foreland. However, the stratigraphic record of the Pipanaco Basin is almost entirely within the subsurface, and no geophysical surveys have been conducted in the region. A high-resolution gravity study has been designed to understand the subsurface basin geometry. This study, together with stratigraphic correlations and flexural and backstripping analysis, suggests that the region was dominated by a regional subsidence episode of *ca.* 2 km during the Miocene–Pliocene, followed by basement thrusting and *ca.* 1–1.5 km of sediment filling within restricted intermontane basin between the Pliocene–Pleistocene. Based on the present-day position of the basement top as well as the Neogene–Present sediment thicknesses across the Sierras Pampeanas, which show slight variations along strike, sediment aggradation is not the most suitable process to account for the increase in the topographic level of the high-elevation, close-drainage basins of Argentina. The close correlation between the depth to basement and the mean surface elevations recorded in different swaths indicates that deep-seated geodynamic process affected the northern Sierras Pampeanas. Seismic tomography, as well as a preliminary comparison between the isostatic and seismic Moho, suggests a buoyant lithosphere beneath the northern Sierras Pampeanas, which might have driven the long-wavelength rise of this part of the broken foreland after the major phase of deposition in these Andean basins.

INTRODUCTION

The Pipananco Basin is one of the largest endorheic basins in South America, developed in the northern part of the Argentine broken foreland province (Fig. 1). Today, the Pipanaco Basin is a flat, high-elevation (*ca.* 1000 m a.s.l.) perched alluvial depocenter. Regional correlations suggest that Mio–Pliocene strata underlie the modern landscape (Bossi & Muruaga, 2009), which would have overstepped the present-day boundaries of the basin. Recent studies have proposed that these Mio–Pliocene sedimentary depocenters were fed from the Puna Plateau (e.g. Fiambalá basin, Carrapa *et al.*, 2006, 2008) or from the Main Cordillera (Tripaldi *et al.*, 2001) during the major pulse of Andean deformation between *ca.* 10 and 6 Ma, constituting a typical foreland basin system (e.g. Decelles & Giles, 1996). From the Pliocene to present-day, the entire region must have risen in elevation by a combination of sediment accumulation in closed-drainage basins and deep-seated geodynamic processes (Strecker *et al.*, 2009). The Pipanaco Basin currently shows a significant step in the long-wavelength topography (Fig. 1) between the depressed southern Sierras Pampeanas to the South and the high Puna plateau to the North (Whitman *et al.*, 1996; Allmendinger *et al.*, 1997; Dávila *et al.*, 2005).

The rise of basin elevation and sediment accumulation in the broken foreland, including in the Pipanaco basin, might, in part, be generated by sedimentary aggradation within closed-drainage basins (e.g. Strecker *et al.*, 2009, and references therein). No flexural quantifications, however, have tested the influence of shortening and tectonic loading in the generation of accommodation space. The aggradation hypothesis does not predict a strong correlation between the sedimentary thicknesses and the coeval

Correspondence: Federico M. Dávila, Centro de Análisis de Cuencas, CICTERRA-UNC, FCEFyN, Ciudad Universitaria, Av. Velez Sarsfield 1611, Córdoba, 5016, Argentina. E-mail: fmdavila@efn.uncor.edu

[1]Present address: Earth Sciences, University College London Gower Street London WC1E 6BT United Kingdom

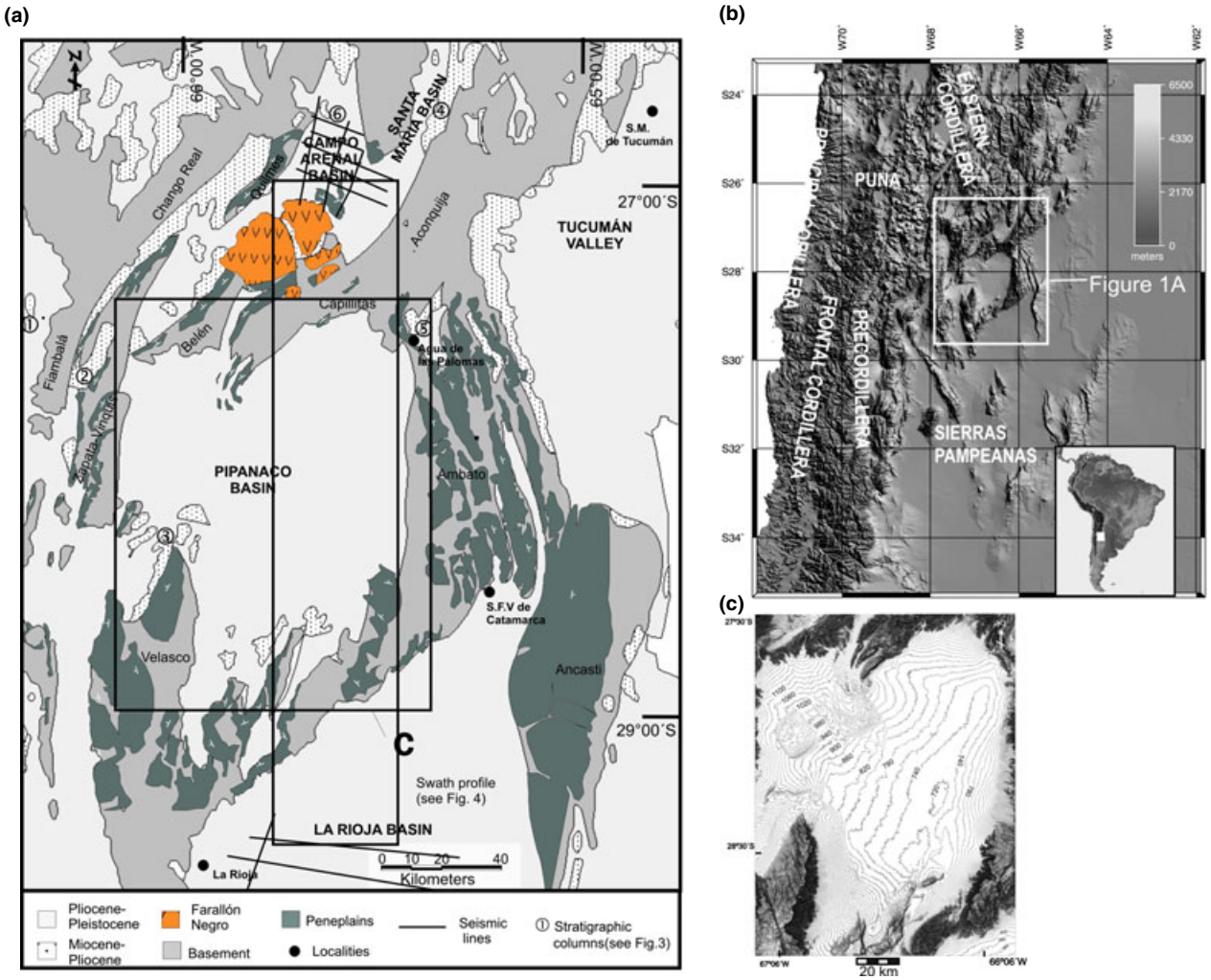

Fig. 1. (a) Geological map of the Pipanaco basin and locations of simplified stratigraphic columns shown in Fig. 3, identified by numbers (after Bossi & Muruaga, 2009). (b) Elevation contour line map of the study area, (c) Digital elevation model (DEM) of the study area and morphotectonic domains of the Central Andes.

tectonic loads, especially in intermontane basins. If the mountain barriers (ranges) were effective and not defeated by fluvial incision, an endorheic system has developed; the depocenter might have accumulated sediments without any flexural subsidence.

Unfortunately, the Pipanaco basin lacks well-exposed stratigraphic records (Bossi *et al.*, 1999), as the strata have not been deformed and hence, occur only within the subsurface. Associated exposures have been intensely studied in the surrounding regions (Jordan & Allmendinger, 1986; Strecker *et al.*, 1989; Bossi *et al.*, 2000; Fisher *et al.*, 2002; Ramos *et al.*, 2002; Sobel & Strecker, 2003; Dávila & Astini, 2003, 2007; Dávila *et al.*, 2005; Carrapa *et al.*, 2008; Mortimer *et al.*, 2007; Bossi & Muruaga, 2009; Nóbile & Dávila, 2011; among others). In addition, we have access to geophysical subsurface data from nearby areas (e.g. Febrer *et al.*, 1982; Fisher *et al.*, 2002; Cristallini *et al.*, 2004; Mortimer *et al.*, 2007; Mcglashan *et al.*, 2008; Gimenez *et al.*, 2009) that support and complement our field and gravity observations.

The aim of this contribution was to integrate the available geological and geophysical information from surrounding regions with new information from the Pipanaco basin to interpret the basin's evolution as well as to provide an alternative explanation for the formation of the high-elevation basins that developed in the northern part of the Argentine broken foreland. Our geophysical observations are based on an analysis of gravity anomalies. We also analyse and compare the long-wavelength topography between the northern and southern Sierras Pampeanas broken foreland (Whitman *et al.*, 1996; Dávila *et al.*, 2005) including the timing and likely causes of these elevation changes along strike, which will contribute to the recent debate on plateau uplift in the Andes (see Barnes & Ehlers, 2009).

GEOLOGICAL SETTING

The studied region is located between 27°30′–28°30′S and 66°30′–67°W, in the northern part of the Sierras Pampeanas broken foreland (Fig. 1), which at these latitudes, represents the easternmost topography of the

Andean orogen. To the west, it binds the Fiambalá-Famatina basement thrust belt (Dávila & Astini, 2007) (Fig. 1), which is considered to be the main topographic load at these latitudes (Dávila, 2003).

Within the broken foreland, the Pipanaco basin is a high-elevation active basin (*ca*. 1000 m a.s.l.), surrounded by *ca*. 2000 m high mountain peaks that expose basement rocks (Fig. 1). The basin is clearly distinguished as a topographically high feature when compared with the La Rioja basin (Fisher *et al.*, 2002), immediately to the south, and the Tucumán Basin (Cristallini *et al.*, 2004) to the east, both of which lie below 350 m a.s.l. (Fig. 1). Large-scale mapping surveys partly cover the studied region (e.g. González Bonorino, 1950, 1972; Socic, 1972, 1973), but few modern and detailed studies have been undertaken.

The mountain system surrounding the basin is formed by doubly vergent basement ranges (Ramos *et al.*, 2002; Cristallini *et al.*, 2004), which are limited by high-angle thrusts, with offsets between 200 and 4000 m. The accommodation space within the intervening basins (intermontane basins) has been explained by a combination of flexural loading, topographic barriers and dynamic topography (Dávila *et al.*, 2005, 2007, 2010). However, the precise mechanism is still a topic of debate.

Miocene to Pleistocene strata deposited on top of the Proterozoic-Paleozoic crystalline basement forms the basin fill (Fig. 1), which is described in the following section.

STRATIGRAPHY

Crystalline basement substrate

The basement of the Pipanaco basin exhibits upper Proterozoic-Paleozoic schists, gneises, amphibolites, migmatites, granulites and granites (see Hockenreiner *et al.*, 2003; Dahlquist *et al.*, 2006; Verdecchia *et al.*, 2007; Büttner, 2009; among others). The basement is widely exposed along and across strike (Figs 1–3) and controls the thrusting style and Andean deformation of the region (Ramos *et al.*, 2002).

According to published seismic sections, the top of the basement underlying the basins occurs at depths between *ca*. 2000 m. a.s.l. to the north (Campo del Arenal, Mortimer *et al.*, 2007) and *ca*. 3000 below sea level to the south (La Rioja Basin, Fisher *et al.*, 2002) (Fig. 4).

Pre-Andean cover

Upper Paleozoic and Mesozoic records are poorly represented in the northern Sierras Pampeanas. A very thin Upper Paleozoic succession (González Díaz, 1970; Bossi & Muruaga, 2009) crops out at the Cébila gorge, southeast of the Pipanaco basin. These exposures are related to late-stage accumulations within glacial paleovalleys (Astini, 2009), which are capped by the more extensive Permian red beds of the Paganzo Basin (Salfity & Gorustovich, 1983). No Mesozoic rocks have been described along the exposed rims of the basin. One hundred kilometres to the south, in the central Sierras Pampeanas, Cretaceous strata locally lap onto basement rocks (Caminos, 1979); these have been interpreted as rift-related deposits (Fisher *et al.*, 2002). The nearest strata within the Velasco range are tens of metres thick and are composed of calcareous sandstones, which bear dinosaur eggs (Tauber, 2007).

Miocene and Pliocene Andean strata

The clearest stratigraphic manifestation in the region, which constitutes a marker for subsurface correlation in this work, is the occurrence of thick synorogenic coarse-grained successions lapping onto the basement (Figs 1–3). These are thick alluvial strata (*ca*. 2000 m), mainly of Miocene to Pliocene age, that developed on an ancient flattened planation surface that formed on a crystalline basement (Figs 1 and 2) and is known as the 'Pampean peneplain' (Jordan *et al.*, 1989). Figure 3 synthesizes the

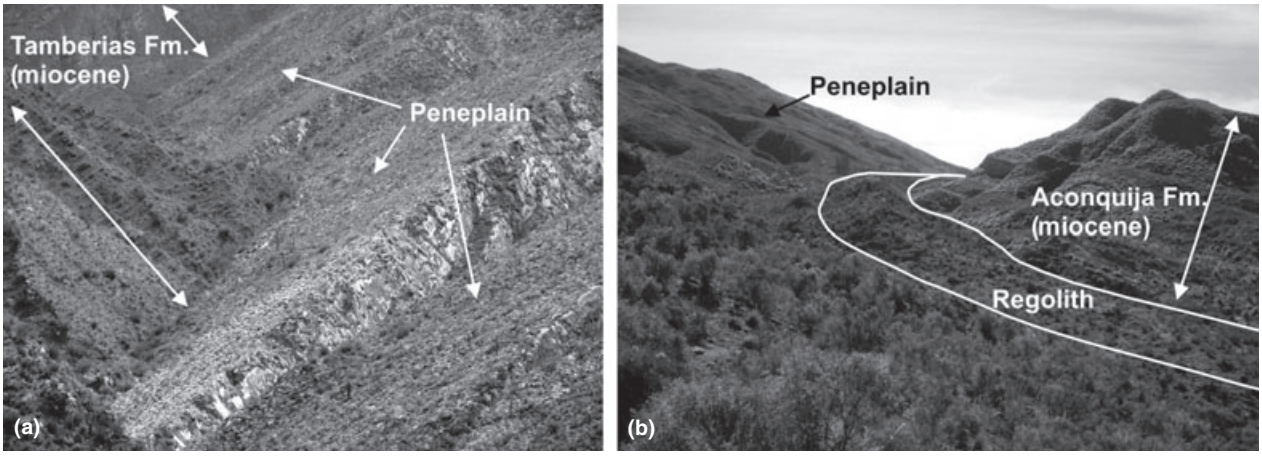

Fig. 2. Basement (Pampean peneplain) in the western (a) and eastern (b) Sierras Pampeanas broken foreland. Notice that the peneplain surface is overlain by a thick regolith layer and that the Miocene units rest subparallel on the paleosurface.

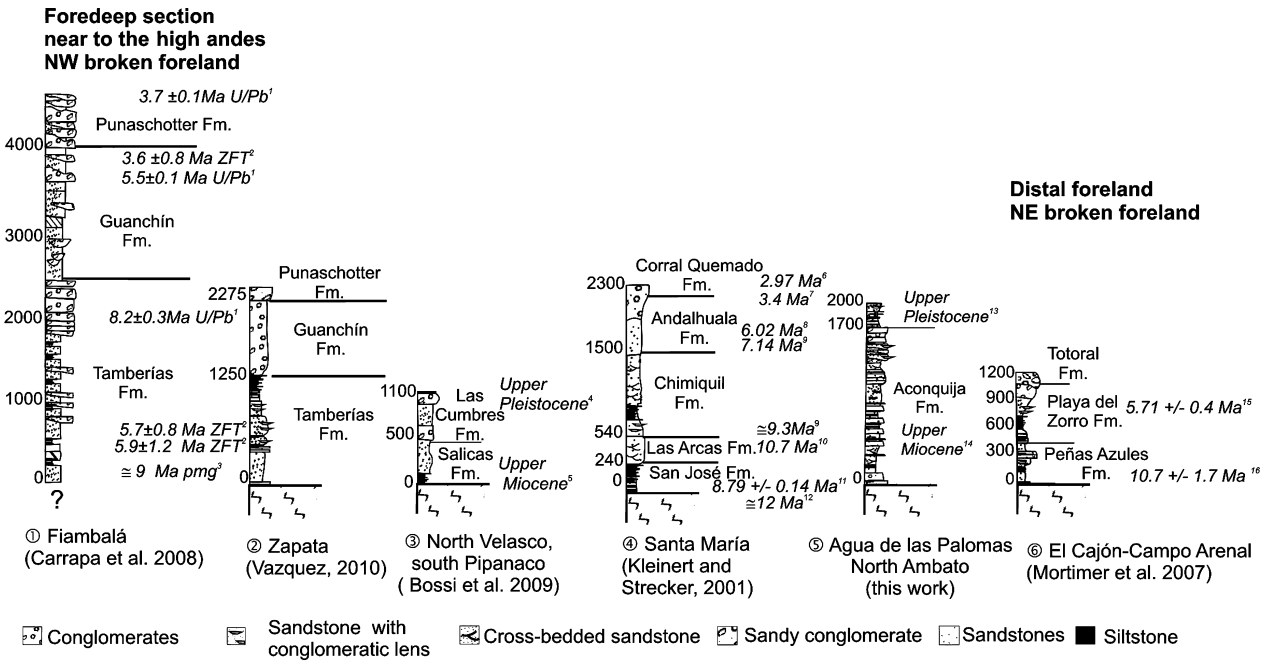

Fig. 3. Neogene stratigraphy along and across the northern Sierras Pampeanas broken foreland, between the Famatina and the Ambatos ranges (see location of columns and ranges in Fig. 1). Note the Mio–Pliocene in the more distal foreland is around 2 km thick. 1 Carrapa *et al.*, 2008; 2 Tabbutt, 1986; 3 Reynolds, 1987; 4 Bossi *et al.*, 2009; 5 Tauber, 2005; 6 Strecker *et al.*, 1989; 7 Strecker *et al.*, 1984; 8 Marshall *et al.*, 1979; 9 Latorre *et al.*, 1997; 10 Caelles *et al.*, 1971; 11 Spagnuolo *et al.*, 2010; 12 Gavriloff & Bossi, 1992; 13 Duarte, 1997; 14 Nasif *et al.*, 2007; 15 Bossi *et al.*, 1997; 16 Strecker, 1987. ZFT, zircon fission track, pgm: magnetostratigraphy, U-Pb geochronology. The rest of the ages are Ar-Ar and K-Ar dates.

likely correlations between the units; Table 1 shows the ages and most accurate constraints.

(1) The intermontane Fiambalá Basin, NW of the Pipanaco basin, contains *ca.* 2–4 km of Neogene strata. Miocene and Pliocene fluvial-alluvial successions are known as the Tamberías and Guanchín Formations (Carrapa *et al.*, 2006; Vázquez, 2010). These are unconformably covered by the Plio-Pleistocene Punaschotter Conglomerates (Penk, 1920) (columns 1 and 2 in Fig. 3). The Mio-Pliocene units have been interpreted as a proximal foreland depozone, and are related to the uplift and loading of the Famatina range (Dávila & Astini, 2007).

(2) To the south, exposed Neogene strata cover an area of *ca.* 1 km^2 in the northernmost Velasco Range. These strata (*ca.* 1.1 km thick) have been described as the fluvial Salicas Formation and the proximal alluvial conglomerates of Las Cumbres Formation (Socic, 1972; Bossi *et al.*, 2007, 2009) (column 3 in Fig. 3).

(3) To the north, the Mio-Pliocene crops out in two basins: The Cajón-Campo del Arenal and the intermontane Santa Maria Basins. The Hualfín (Muruaga, 1998, 2001a, b; Bossi *et al.*, 1999), San José, Las Arcas, Chiquimil, Andalhuala, Corral Quemado and Yasamayo Formations comprise the local stratigraphy (Galván & Ruiz Huidobro, 1965; Bossi & Palma, 1982) (column 4 and 6 in Fig. 3). These were also interpreted as alluvial deposits.

(4) On the eastern slope of the Aconquija range, 5 km north from the Agua de Las Palomas village (Fig. 1), Mio-Pliocene deposits are *ca.* 1600 m thick. These are known as the Aconquija Formation (González Bonorino, 1950; Nasif *et al.*, 2007) (column 5 in Fig. 3) and represent an upward progression of the sedimentation from distal to proximal alluvial fans. Quaternary conglomerates lapping unconformably onto these strata represent the first records of intermontane sedimentation in the region.

This contribution will refer to these units exposed in the northern Sierras Pampeanas as Miocene-Pliocene, thus avoiding their local formational names.

Industry seismic reflection sections across the nearby intermontane valleys (Campo del Arenal and La Rioja basins, Fig. 1) have shown 'Cenozoic' strata that are *ca.* 2000–3000 m thick (Fisher *et al.*, 2002; Dávila *et al.*, 2007; Mortimer *et al.*, 2007; Bossi & Muruaga, 2009). Only the subsurface Campo del Arenal reflectors can be correlated with stratigraphic exposures. To the south, in the Velasco and Brava ranges, thin (<200 m) Middle Miocene paleosoil horizons (Ezpeleta *et al.*, 2006; Dávila *et al.*, 2007) extend uncorformably over basement rocks or Paleozoic-Mesozoic cover.

Neogene volcanism

The formation of the broken foreland has been largely related to slab shallowing (Ramos *et al.*, 2002). Retroarc volcanic broadening affected the Sierras Pampeanas during the Miocene and continued through the Pliocene (Kay *et al.*, 1988; Sasso & Clark, 1998; Kay & Mpodozis,

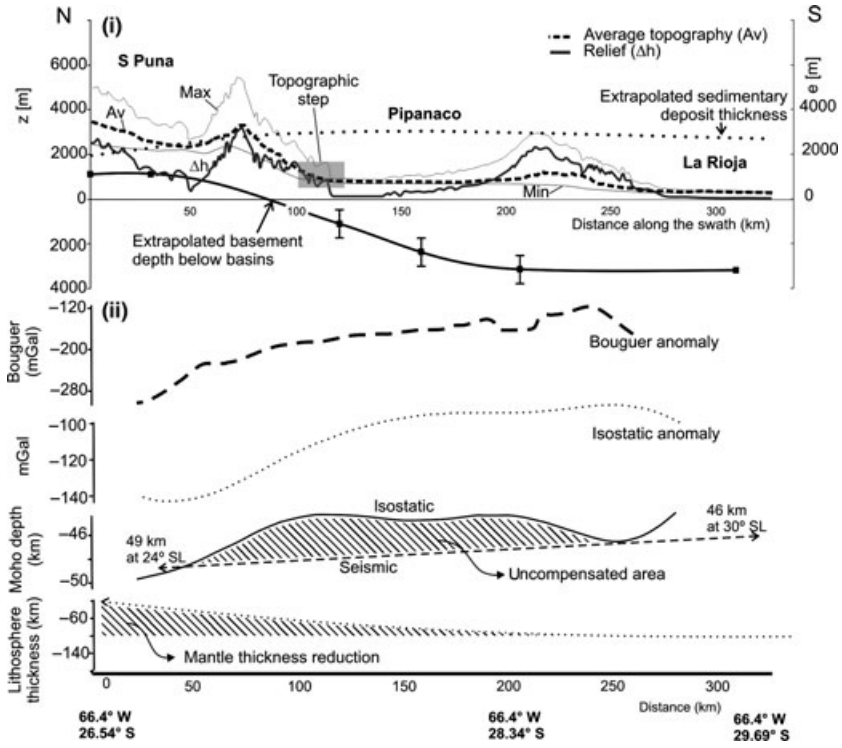

Fig. 4. (i) North-South (azimut 0º) topographic swaths along 66.4°, 350 km length and 150 km wide, from 26.54 to 29.69 SL. Z is the altitude with respect to the sea level and e is thickness of Andean sedimentary successions, both in metres. Thick dashed line is average topography (Av); thick grey solid line is relief (Dh); thin lines are maximum (Max, solid line) and minimum (Min, dashed line) topographies. Basement top position below the basins is the solid line with squares and the sedimentary thickeness of Andean synorogenic strata (e[m]) is the spaced dashed line. The extrapolated basement depth curve below the sedimentary basins were estimated using the interpretations by Mortimer *et al.* (2007), in Campo Arenal southward from the S Puna, the gravity analysis in Pipanaco (this work) and by Fisher *et al.* (2002) in the La Rioja Basin. Note the error bars estimated from gravity inversion models in the Pipanaco Basin (see further details in the Appendix: Fig. S3a, b). The exhumed basement rocks from hilly areas were not considered (exposed by tectonics). Note that the minimum topography of the modern basin levels does not correlate with the sediment thickness curve, i.e. it is not observed as a good matching between filling and vertical aggradation with the topographic levels in the basins. The basement top position, in contrast, shows a strong correlation with the topographic curves. (ii) Regionals Bouguer and isostacy anomalies along the northern Sierras Pampeanas. The bottom curves show the moho depth and lithosphere thickness. Note the uncompensation area that results from the comparison between the gravity and seismic (Whitman *et al.*, 1996; Mcglashan *et al.*, 2008) crustal thicknesses. The extrapolation in the seismic moho follows the Whitman *et al.* (1996) crustal structure. The northward mantle-lid thinning (from Whitman *et al.*, 1996) agrees with the development of the Puna plateau and the high altitude of the N borken foreland.

2002; Ramos *et al.*, 2002; Dávila *et al.*, 2004; Davila, 2010). The Farallón Negro Complex, north of the Pipanaco basin in the Sierra de Belén (Fig. 1), is probabaly the largest volcanic field within the Argentine foreland. It has an area of >250 km^2 and is located *ca.* 1500 m above the Pipanaco basin level. Basalts, rhyolites and associated volcanoclastic successions, intruded by world-class porphyry copper-gold bearing bodies, form the complex. The complex was originally emplaced at shallow depths (2.5–3.5 km), intruding basement rocks (Llambías, 1970; Sasso & Clark, 1998; Bain, 2001). The *ca.* 12.5 Ma age of the complex (Sasso & Clark, 1998; Halter *et al.*, 2004) is contemporeous, with the oldest synorogenic strata described above. As Pliocene alluvial conglomerates overlay the Farallón Negro rocks, the denudation of the subvolcanic field would have occurred between the volcanic crystallization and sedimentation ages (Mio-Pliocene). This interpretation is consistent with apatite fission-track ages of *ca.* 7.6–4.2 Ma (Coughlin, 2000) in the Sierra de Capillitas, located a few kilometres east of Farallón Negro and at approximately the same elevation.

Quaternary

Pleistocene deposits are evidence of a strong west-east asymmetry in the sedimentary environments. They are represented by coarse alluvial fans, exposed in piedmont terraces adjacent to the uplifted ranges, and eolian sand dunes (Tripaldi *et al.*, 2005) at the NW edge, ephemeral fluvial deposits in the central part and saltpans and playa-lakes, known in the local literature as the 'Salar de Pipanaco' along the eastern border. To the east, the base of the Quaternary lies within the subsurface, whereas along the west and southwest border of the basin, it is exhumed and slightly tilted. At the base of the Ambato range, bounding the Pipanaco basin to the east, colluvial sediments affected

Table 1. Chronological constraints of Neogene and Quaternary strata

Section	Age	Method	Author	Fm.
Fiambalá (*Carrapa et al., 2008*)	3.7 ± 0.1 Ma	U/Pb	Carrapa *et al.*, 2008;	*Punaschotter Fm.*
	3.6 ± 0.8 Ma	Zircon fission-track ages	Tabbutt, 1986;	*Guanchín Fm.*
	8.2 ± 0.3 Ma	U/Pb	Carrapa *et al.*, 2008;	*Guanchín Fm.*
	5.7 ± 0.8 Ma	Zircon fission-track ages	Tabbutt, 1986;	*Tamberías Fm.*
	5.9 ± 1.2 Ma	Zircon fission-track ages	Tabbutt, 1986;	*Tamberías Fm.*
	≈9 Ma	Paleomagnetic (pmg) data	Reynolds, 1987;	*Tamberías Fm.*
North Velasco, south Pipanaco (*Bossi et al., 2009*)	Upper Pleistocene	Pampean peneplain	Bossi *et al.*, 2009;	*Las Cumbres Fm.*
	Upper Miocene	Vertebrate's record	Tauber, 2005;	*Salicas Fm.*
Santa María (*Kleinert and Strecker, 2001*)	2.97 ± 0.6 Ma	Fission-track age	Strecker *et al.*, 1989;	*Corral Quemado Fm.*
	2.97 Ma–3.4 Ma	Fission-track age	Strecker *et al.*, 1984, 1989;	*Corral Quemado Fm.*
	6.02 Ma		Marshall *et al.*, 1979;	*Andalhuala Fm.*
	Between 7.4 and ≈9.3 Ma	Based on K-Ar ages and magnetostratigraphic data obtained by Butler *et al.* (1984) and complemeted by Latorre *et al.*, 1997;	Bossi *et al.*, 1997;	*Chimiquil Fm.*
	10.7 ± 0.3 Ma	Andesitic volcanic rocks	Caelles *et al.*,1971;	*Las Arcas Fm.*
	≈ 13–12 Ma	Biostratigraphic data	Gavriloff & Bossi, 1992; Bossi *et al.*, 1997;	*San José Fm.*
Agua de las Palomas North Ambato (*this work*)	Upper Pleistocene	Vertebrate's record	Duarte, 1997;	Quaternary deposits
	Upper Miocene-Pliocene	Vertebrate's record	Nasif *et al.*, 2007;	*Aconquija Fm.*
El Cajón-Campo Arenal (*Mortimer et al., 2007*)	–			*Totoral Fm.*
	5.71 ± 0.4 Ma		Bossi *et al.*, 1997	*Playa del Zorro Fm.*
	10.7 ± 1.7 Ma		Strecker, 1987	*Peñas Azules Fm.*

by historical and recent earthquake ruptures (Eremchuck, 1984) are locally observed. The depositional asymmetry may be related to regional gradients due to eastward alluvial progradation (as suggested by the drainage systems), although a subsidence control cannot be discarded (see below).

Within the Ambato range, upper Pleistocene loess-rich successions and mudstone deposits bearing glyptodonts (Duarte, 1997) rest subhorizontally, lapping onto Mio-Pliocene sediments, basement rocks (Fig. 6) and cataclastic zones, providing an important constraint on the major deformation and uplift stage in this region.

METHODS

This study employed three main approaches: (1) gravity analysis to determine the subsurface basin geometry and structural controls in the Pipanaco basin, (2) stratigraphic correlation along and across strike to understand the sedimentary fill and to recognize depositional sequences to be tested by (3) backstripping and flexural modelling to quantify the accommodation by compaction and tectonic loading. A complementary topographic analysis of the surface and substrate of the Pipanaco basin and of the nearby basins complements these basin studies, to analyse the likely controls on the development of high-altitude basins of the northern Sierras Pampeanas.

The gravity analysis was designed to separate and analyse anomalies and anomaly signals, as well as to construct a three-dimensional subsurface model of the basin. The raw data was corrected using traditional approaches to isolate the Bouguer anomaly. Spectral, Euler deconvolution and analytical signal analysis (see Appendix) provide information about the density variations that can be associated with lateral changes in rock composition, intrusions, faults, etc. The errors involved in the depth calculations are shown as a function of the gravity effect and density variations (Appendix). Note that the largest error in the basement depth within the central part of the basin is ±800 m. Gravity studies in the Rioja basin (Gimenez *et al.*, 2009), south of the Pipanaco basin, assisted us in evaluating input parameters for the gravity model of the Pipanaco basin and in correcting the preferred densities and interpretations. Seismic data from La Rioja Basin serve to correct and correlate gravity information (Gimenez *et al.*, 2009). Seismic refraction reports gathered by YPF (Yacimientos Petrolíferos Fiscales, Argentina, released unpublished report, 1982) in the Pipanaco basin were also used to estimate sedimentary velocities at *ca.* 2800 m/s for the upper layers, roughly corresponding to *ca.* 2300 m of sedimentary fill. Velocities of *ca.* 5500 m/s were proposed for the crystalline basement. These velocities were transformed into densities using a correlation with the Brocher (2005) approach, and support the estimations obtained from the gravity analysis.

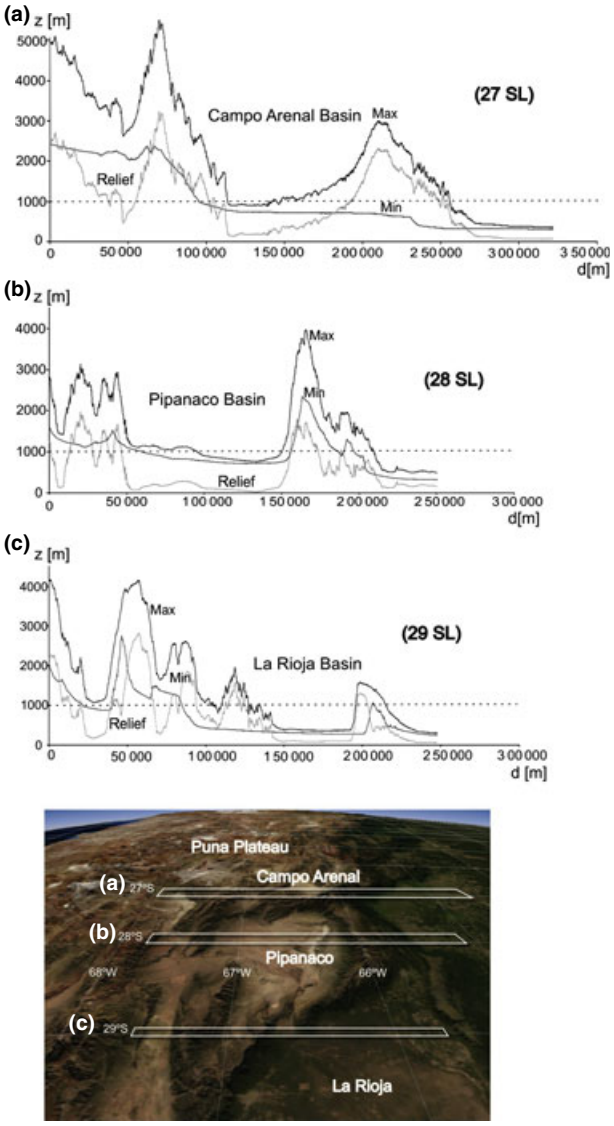

Fig. 5. Quaternary strata on the eastern flank of the Ambato range lying subhorizontally on a tilted surface of basement (Pampean peneplain). Considering the Mio–Pliocene strata were rotated together with the peneplain, and this relation suggests that major basement deformation and exhumation occurred between Pliocene and Late Pleistocene times.

The densities used to construct a 2D gravity model were estimated from seismic refraction data and the surface geology. A three-layer basin model was adopted, including (a) a low-density sediment layer (Quaternary) with a density of *ca.* 2.2 g/cm^3, (2) an underlying sedimentary layer of <2.6 g/cm^3, and (3) crystalline basement with a density of >2.6 g/cm^3. The gravity influence of the basement was filtered to estimate the geometry of the basin substrate and the maximum sedimentary thickness, i.e. by extracting the signals with densities <2.6 g/cm^3. Note that the errors in estimating the layer depths are directly associated with the density chosen for each layer. A difference of *ca.* 0.1 g/cm^3 reproduces depth differences in the order of *ca.* 800 m.

The gravity results were compared with the exposed stratigraphy (from geological compilations and fieldwork performed in the Pipanaco basin and the surrounding Fiambalá/Zapata, Velasco, Ambato and Belén/Capillitas ranges, see Fig. 1). Given that the local stratigraphy is essentially Neogene over basement, the top of basement would basically be depicting the Neogene depocenter geometry.

Backstripping and flexural modelling were conducted using the free-access programmes of Nestor Cardozo (homepage.mac.com/nfcd/work/programs.html). Input data and constants used are shown and explained in the Appendix. These results have been compared with the sedimentary thicknesses recorded by gravity data to detect likely anomalies in accommodation.

At the scale of the entire Sierras Pampeanas province, topography was analysed using Digital Elevation Models (DEM) of the shuttle radar topography mission (SRTM). A 70-km width swath-topographic profile was constructed at *ca.* 66°W, from the southern edge of the Puna to the Rioja basin (crossing the Campo del Arenal and Pipanaco basin, Figs. 1, 4), which shows maximum, minimum and mean elevations as well as relief (Note that the term relief refers to a difference in height, whereas elevation and altitude refer to height above a datum, normally mean sea level). Along this swath, the location of the basement top beneath the intermontane basins and the Neogene sedimentary thicknesses were estimated and extrapolated to evaluate relationship between topography and basin substrate and how the sedimentary aggradation drives topography (elevation of the basin level) within intermontane basins similar to Pipanaco (Fig. 4). Three west–east 40-km width topographic swaths were also constructed along latitudes *ca.* 27°, 28° and 29° S (Fig. 5) to complement the regional north–south swath. Note that the 28° S swath covers the Pipanaco basin. These W–E swaths depict the relationships between the ridgelines relative to the elevation of the basin floors, the topographic variation from north to south and the dimensions and geometry of the intermontane basins. A set of available reflection seismic sections from nearby regions, e.g. La Rioja Basin (Fisher *et al.*, 2002; Dávila *et al.*, 2007), Campo del Arenal basin (Cristallini *et al.*, 2004; Mortimer *et al.*, 2007; Bossi & Muruaga, 2009) and the Tucumán valley (Cristallini *et al.*, 2004) were used to evaluate the subsurface geology north and south of the Pipanaco basin.

RESULTS AND INTERPRETATIONS

Gravity

The residual bouguer anomaly map (Fig. 7) shows the largest negative values in the SE part of the Pipanaco basin; these values correspond to the deepest sedimentary bodies (i.e. with densities <2.4 g/cm^3) (Fig. 8). High-density bodies (>2.7 g/cm^3) with positive gravity signals (using 2.7 g/cm^3 filters) are observed in the western and easternmost parts of the basin. Given the short- to med-

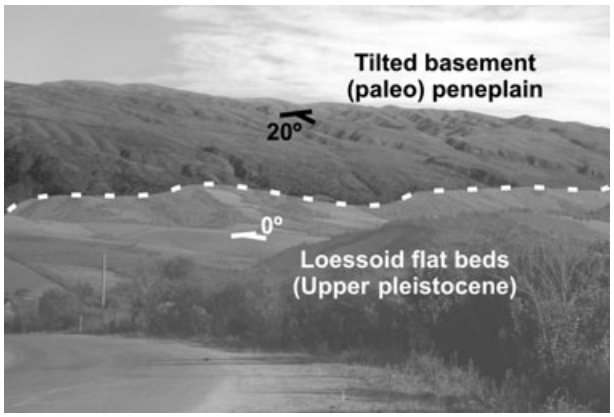

Fig. 6. West-East topographic swaths along (a) 27ºSL (from 27°00′28″S/67°43′47″W to 26°57′40″S/65°09′44″W), (b) 28ºSL (from 28°00′10″S/67°42′60″W to 27°57′20″S/65°10′31″W) and (c) 29ºSL (from 29°01′35″S/67°42′21″W to 28°58′40″S/65°10′4″W), 40 km width. Z [m] is the altitude with respect to sea level in metres. d [m] is the distance along the swaths. Thick solid lines are relief and maximum (Max)/minimum (Min) topography. The 1000-m level is shown as reference. Note that topography increases remarkably northward and the basin floors are close to 1000 m above sea level in a and b, whereas they are below to the south in c. The DEM (view to the north) shows the location of the swaths and analysed basins.

ium-wavelength (10 s of kilometres) signals, these bodies would be located within the uppermost crust (see below).

To calculate the depths to the top of basement and the location of dense bodies within the upper crust (Fig. 8), a three-dimensional gravity inversion was performed on the residual Bouguer anomalies. This inversion shows that the maximum thickness of the sedimentary fill is about 3000–3500 m. Results from a radial power spectrum analysis corroborate the 3D gravity inversion estimation. This analysis calculates the depth to the sources by the slope of the logarithm of the power spectrum as a function of the logarithm of the wave number (see Fig. 9 and Appendix 'Gravity corrections') (B in Fig. 8). Results show a maximum sedimentary signal depth between 2500 and 3000 m (consistent with the results obtained by the 2D model described below). The western edge of the basin, however, shows thicknesses of <1000 m (Fig. 8). Notice that the errors involved in the calculations are in the order of ±800 m (see further details in the methodology). The differences in thickness between the east and west are consistent with unpublished refraction tests (National Oil Company YPF home reports) conducted in the central part of the Pipanaco basin, which predicted *ca.* 2300 m of Cenozoic fill. Values also agree with estimations for the Campo del Arenal, to the north, and to the Rioja basins to

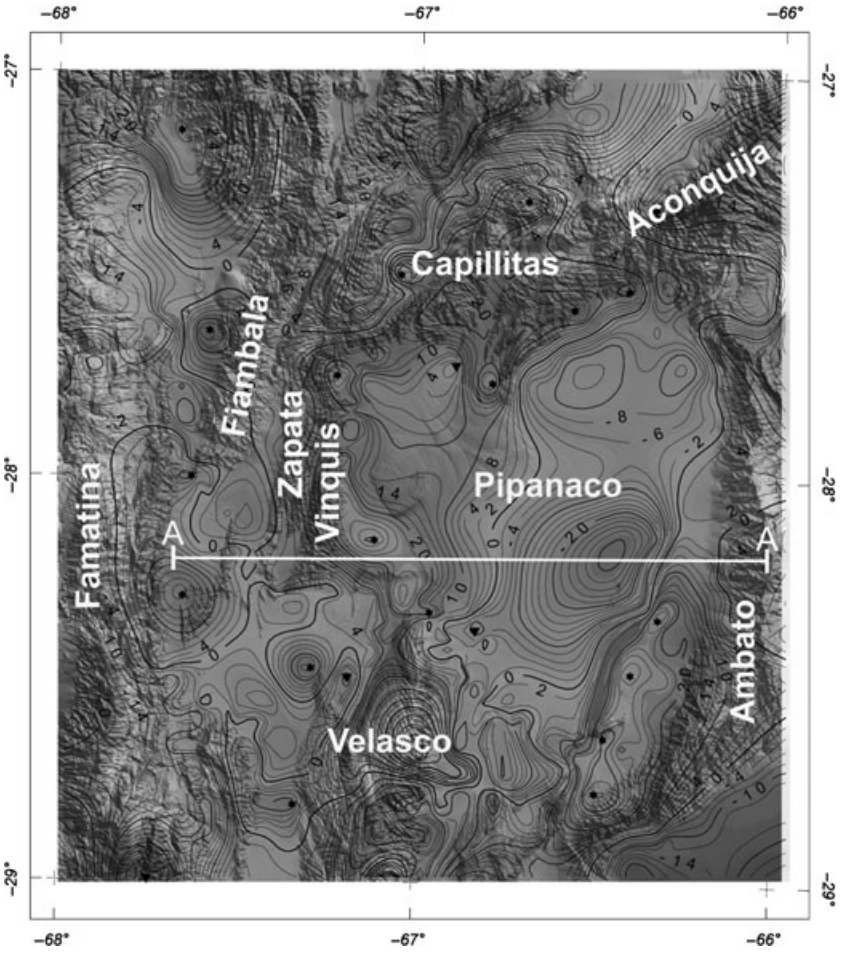

Fig. 7. Residual Bouguer anomaly map overlain on a DEM of the study region. The curve values are in mgals. A–A′ shows the location of the profile depicted in Fig. 10.

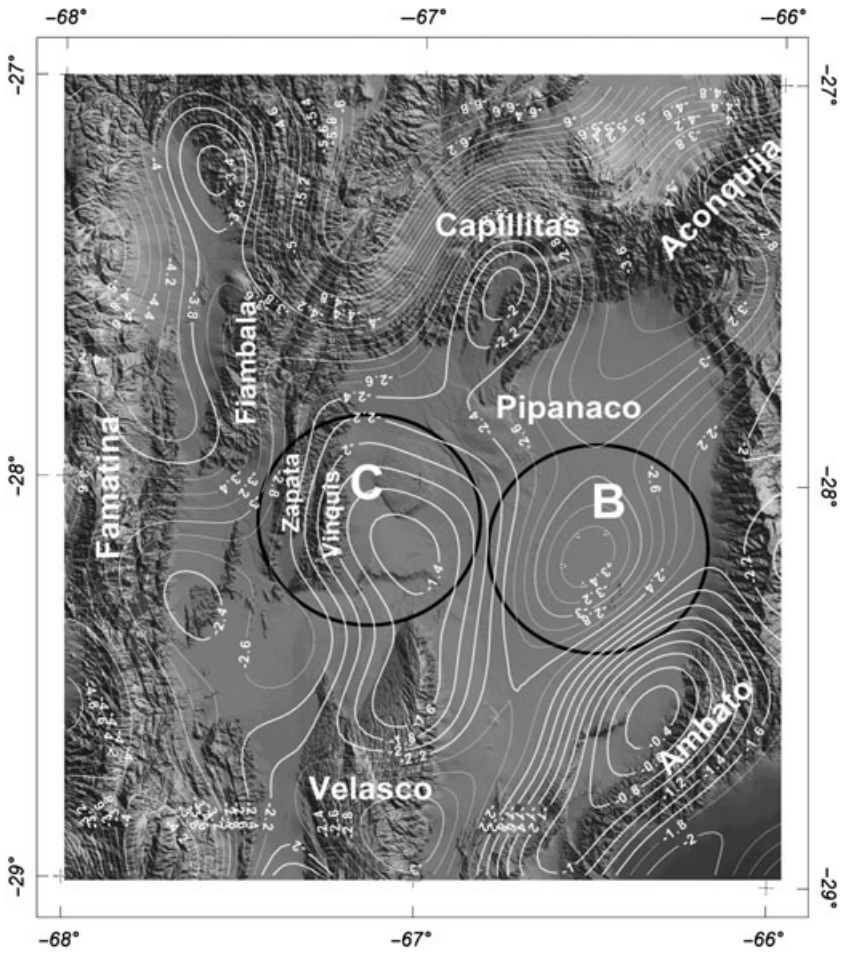

Fig. 8. Geometry of the basement top, obtained by gravity inversion of the residual Bouguer anomaly. Values are in kilometres below the surface. C and B show the location of the radial spectrum depicted in Fig. 9.

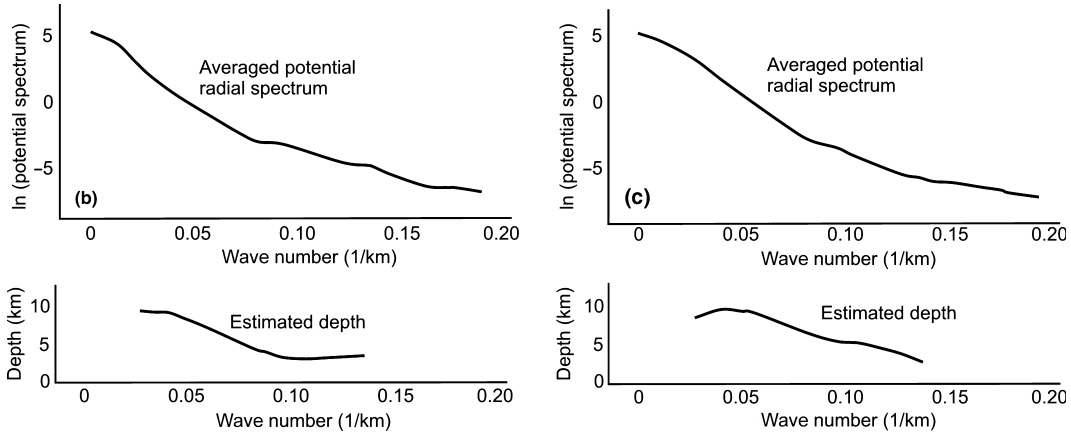

Fig. 9. Radial spectrum curves of the circles shown in Fig. 8 as B and C. The curve B allows estimating the maximum depth of the Pipanaco basin, whereas C calculates the depths of the dense bodies (positive Bouguer anomalies).

the south, where the maximum sedimentary thicknesses are *ca.* 3000 m (similar to Pipanaco). In addition, this model shows that the high-density bodies would be located at *ca.* 5000 m depth (Fig. 9b).

Figure 10 shows the Euler deconvolution solutions used to calculate the variations of the gravity gradient signal. Note that the changes in gravity gradients and positive anomalies practically overlap geographically, and the anomalous density depth values vary between 4 and 8 km below the surface (Fig. 10). These variations are due to abrupt changes in the composition of the substrate, commonly caused by faults or intrusions with densities different from the country rock.

A 2D gravity model (Fig. 11) verifies the residual Bouguer anomaly, the gravity inversion model (Fig. 8) and the Euler deconvolution results (Fig. 10). To better match the gravity model with the measured residual Bouguer anomaly, it was necessary to incorporate dense

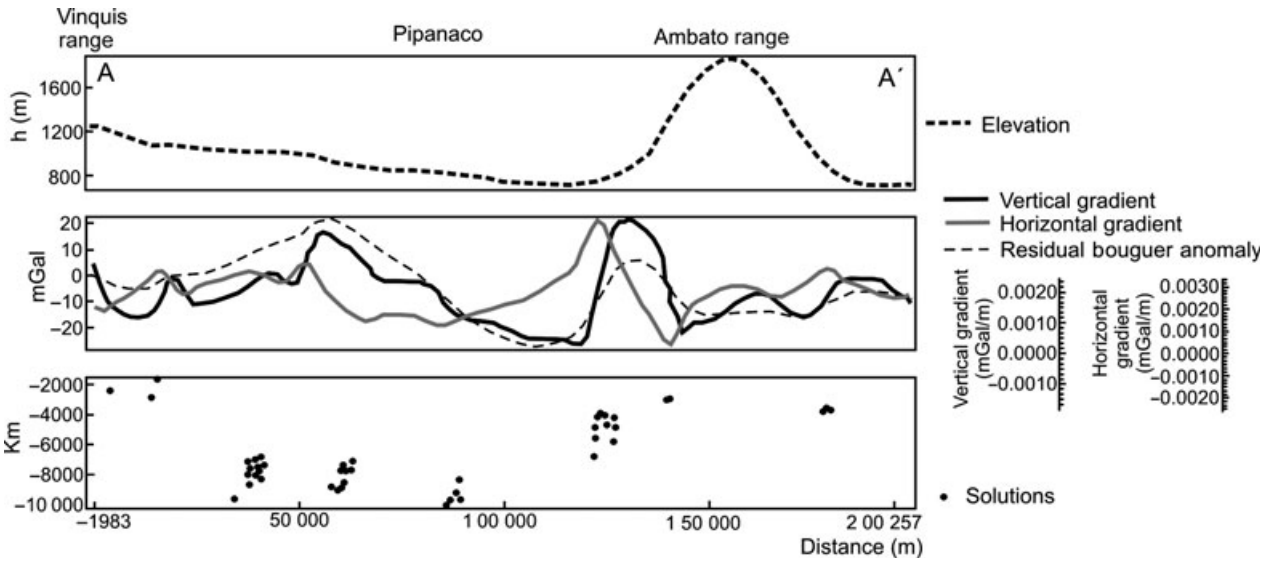

Fig. 10. 2D Euler deconvolution achieved on the residual Bouguer anomaly signal along A–A´ (see location in Fig. 7). A structural index of 0.5 was used in calculations (see text and supplementary data for further details).

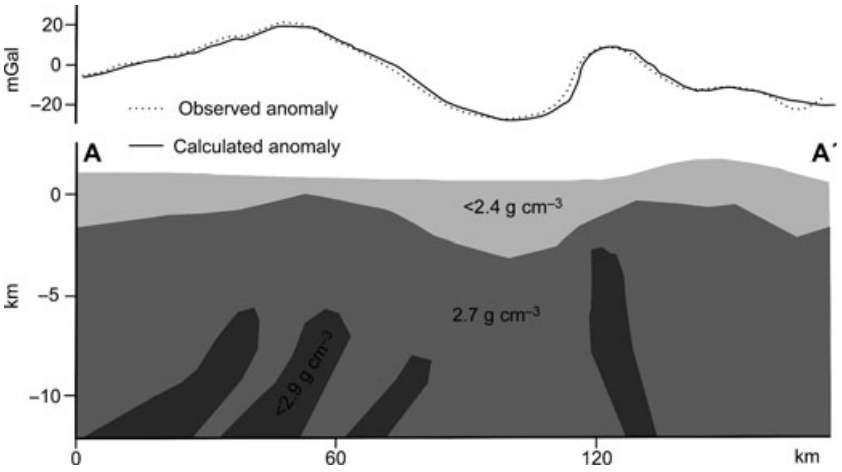

Fig. 11. Upper crustal gravity model along the profile A–A´ (see location in Fig. 6). This proposal agrees with the Bouguer anomalies and the geological observations.

bodies of *ca.* 2.9 g/cm^3. Their location was chosen on the basis of the position of the solutions of the Euler deconvolution and the analytic signal method (Fig. 10 and Appendix). The 2D model is also consistent with the field geology and stratigraphy of the region.

The dense bodies were correlated and modelled as Andean subvolcanic intrusions, analogous to the Farallón Negro complex, which is exposed a few kilometres to the north. According to the Euler deconvolution and the analytical signal (Fig. 10), these bodies would today be located at *ca.* 5 km depth and would have a diameter of *ca.* 10–20 km. As older intrusions (e.g. Late Paleozoic) have not shown clear density contrasts in surface gravity surveys (Martinez *et al.*, 2008), we interpret the dense bodies as being similar to the Cenozoic igneous intrusions exposed to the north (see Fig. 1), which have yielded strong positive gravity signals. A structural alternative similar to that proposed by Alvarado & Ramos (2011) in the southernmost Pipanaco basin, with thrusts in the middle crust, cannot be discarded. However, it is important to notice that this hypothesis requires that the buried thrusts displace high-density (>2.9 g/cm^3) country rocks, which it is not supported by the regional gravity analysis (Fig. 4).

Stratigraphy correlation, backstripping analysis and flexural model

Consistent with the regional geology (see stratigraphy section above), the entire basin fill (i.e. rock densities <2.6 g/cm^3) is interpreted as Miocene or younger.

As suggested by the gravity studies, the largest sedimentary accumulation (*ca.* 3500 m) develops to the E, towards the foothills of the Ambato ranges (Figs. 8, 11, 12). This thickness represents the maximum difference between the mean modern basin elevation and the highest position of the basement top (i.e. rock densities >2.6 g/cm^3). The values, in turn, agree with estimations in La Rioja Basin, where the Miocene to Quaternary is *ca.* 3000 m thick (Fisher *et al.*, 2002; Dávila *et al.*, 2007;

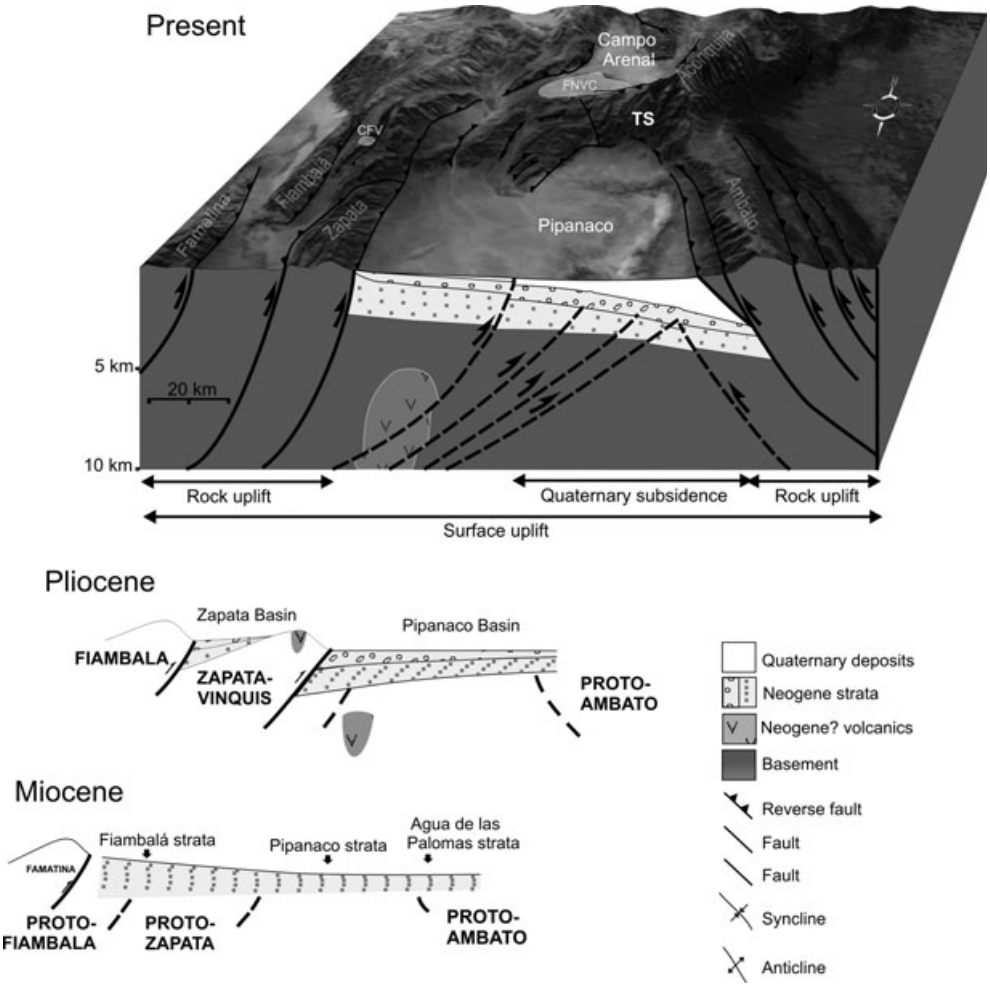

Fig. 12. Evolution of the Pipanaco basin since the Miocene, when the region was an eastward-migrating foreland, to the Plio-Pleistocene, when the uplifting of basement ranges occurred and created isolated and endorreic basin systems, like Zapata and Pipanaco. The block diagram on top shows the Modern scenario, constructed from a northward DEM view, structural interpretations from Mortimer *et al.* (2007), Alvarado & Ramos (2011) and this work. The location of the volcanic bodies is based on correlations and our gravity inversion analyses. TS is the topographic step shown in Fig. 4a. FNVC = Farallón Negro Volcanic Complex, CFV = Cerro Fraile Volcanites. The Miocene and Pliocene reconstructions are based on Dávila & Astini (2007).

Gimenez *et al.*, 2009). Nevertheless, note that the estimation of the basement top location by gravity studies has errors in the order of 800 m.

Given that knowledge of the Pipanaco basin stratigraphy is severely limited by the lack of outcrop, the sedimentary fill was divided into two major sequences (Sobel & Strecker, 2003): the Neogene and the Quaternary. This subdivision is clear and marked by an angular discordance (see Fig. 6), and represented in the exposures by tilted Mio-Pliocene rocks covered by subhorizontal Pleistocene beds. This relationship suggests that the major uplift of the Ambato range would have occurred in the Plio-Pleistocene (Fig. 12). On the basis of the exposed stratigraphy, it is assumed that the Neogene in this part of the northern Sierras Pampeanas has a more or less constant thickness of *ca.* 2000 m. The remaining *ca.* 1000 m in the Pipanaco fill consequently may be Quaternary (Fig. 12). We cannot rule out, at this stage, that part of the deepest sedimentary fill of the Pipanaco basin is formed by thin Upper Paleozoic and/or Cretaceous strata, as evidenced in nearby regions (see above).

If the assumption of a regionally constant thickness of Neogene strata is correct, the comparatively thin strata of the western part of the basin suggests that exhumation removed *ca.* 1000 m of the stratigraphy after the Neogene sedimentation (Fig. 12), preventing Quaternary sediment accumulation on this side of the basin. Along the eastern side, the exact opposite occurred; a significantly larger accommodation space developed, where a remarkable thickness of Quaternary sediments was deposited. This stratigraphic analysis provides the boundary conditions for the basin modelling (discussed below).

Three alternatives were tested to explain the basin surface elevation and sedimentary accommodation across strike: (1) differential sediment compaction, (2) deformation affecting the western sector of the basin, or (3)

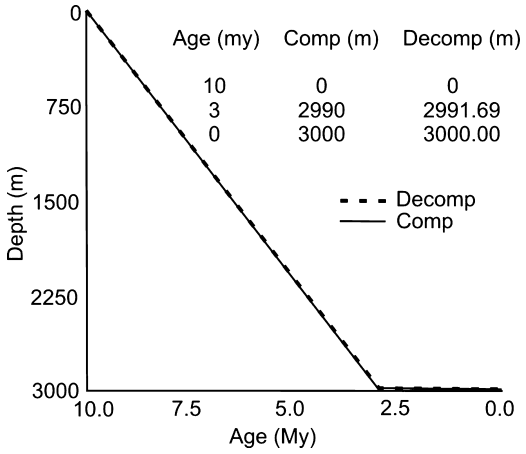

Fig. 13. Decompaction analysis (using OSXBackstrip by Cardozo, N.) that performs a 1D Airy backstripping with exponential reduction of porosity (Allen & Allen, 1990). Note the compacted (Comp) and decompacted (Decomp) curves are imperceptible and overlapped, suggesting no accommodation by compaction of older units during the subsidence history. Stratigraphic and sedimentological data were supplied from surface studies (see stratigraphy chapter). Petrophysical properties (porosity and grain densities) were taken from Allen & Allen (1990).

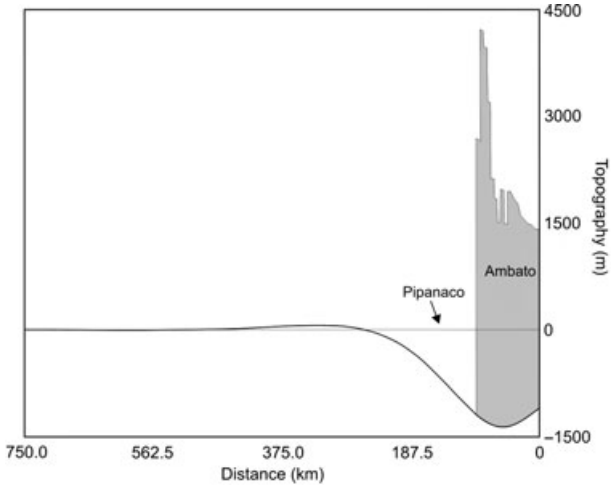

Fig. 14. Flexural model across the Ambato range to estimate the subsidence driven by shortening. We use the infinite-plate analysis in Flex2d (Cardozo & Jordan, 2001). Input parameters were: Young's modulus 70 Gpa, Poisson's ratio 0.25, and effective elastic thickness 40 km. Densities are 3300 kg m^{-3} for the asthenosphere and 2400 kg m^{-3} for the tectonic and sedimentary loads. The load heights were restored from DEM and structural reconstructions. Note that the foredeep has depth of 1200 m and the forebulge is at 230 km from the leading edge of the load and has maximum amplitude of *ca.* 58 m.

flexural subsidence driven by the topographic load located to the east, e.g. the Ambato range.

(1) Our backstripping calculations (Fig. 13) predict compaction of a few metres across the basin (<10 m), whereas the surface relief is *ca.* 200 m (Fig. 1) and the variation of sediment thickness is even larger (Fig. 10). This indicates that the thickness and relief differences between the W and E sectors of the Pipanaco basin (see Fig. 5, 28° SL swath) cannot be attributed to differential compaction across the basin.

(2) The gravity analysis (e.g. Euler deconvolution, see the Appendix) supports the existence of a basement thrust to the west (cluster of sources around 50 km in Fig. 10), which not only explains the regional surface slope toward the east and eastward telescoping of alluvial fans on this side of the basin but also the exhumation and unroofing of the Neogene and lower Quaternary sediments with respect to the eastern side. However, the loading associated with such thrust faulting is not sufficient to produce flexural subsidence in the range of *ca.* 1000 m to account for the Quaternary sediment thickness recorded along the east part of the basin.

(3) The accommodation of the *ca.* 1000 m of Quaternary sediments in the eastern part of the Pipanaco basin was modelled using flexural model (see Fig. 14 and Appendix). The topographic loading by the Ambato range reproduces *ca.* 1 km of flexural accommodation along the eastern border of the Pipanaco basin, consistent with the estimated Quaternary deposits preserved in the subsurface (Fig. 8, elastic parameters used in the flexural model are discussed in the Appendix).

Topography

The N–S swath profile (Fig. 4), as well as the three W–E swaths located at the Puna-Sierras Pampeanas boundary, the Pipanaco basin, and southern Sierras Pampeanas, clearly depicts a remarkable southward reduction in the maximum and minimum altitudes and in the relief (difference between maximum and minimum topography). Towards the north of the profile, a zone with steep slopes divides two wide zones of low relief (at 50 km and 100 km along the profile of Fig. 4). This zone is associated with a clear step in minimum altitudes from *ca.* 2000 m to *ca.* 500 m. The average elevation curve also shows a sharp step to the north of the Pipanaco basin (Av in Fig. 4), with altitudes between 3500 m to the N and 400 m to the S (Av in Fig. 4). Note that this step is >100 km south of the southernmost Andean plateau boundary (Puna in Fig. 1). The relief (Δh) is *ca.* 4000 m (Fig. 4), which probably represents the largest relief along the foreland. This topographic step in the Sierras Pampeanas is located at the same spot where low-temperature thermochronology yielded the youngest cooling ages in the broken foreland, <8 Ma (Coughlin, 2000).

Two additional curves were plotted in Fig. 4 to compare the topography with the sedimentary thickness variations and the depth of basement along strike. The sedimentary thicknesses vary between *ca.* 1 and 3 km, whereas the top of the crystalline basement occurs at *ca.* 2000 m above sea level (a.s.l.) in the Campo del Arenal to the north, *ca.* 2700 m below sea level (b.s.l.) in La Rioja basin to the south and *ca.* 3000 m b.s.l. in the Tucumán basin to the east (Fig. 4), i.e. a difference of *ca.* 5700 m between N and S.

DISCUSSION

Geological and geophysical observations suggest that the Pipanaco basin experienced two major filling stages during the Neogene and the late Pleistocene. A significant basement-thrusting episode separates the depositional stages, which differ substantially. Although the Neogene basin fill would have overstepped the modern landscape of the Sierras Pampeanas to the E (as evidenced by Miocene successions exposed on the east flank of the Ambato range and further east, in the subsurface of the Tucuman Valley), Quaternary sediments were clearly deposited in restricted intermontane depocenters associated with basement deformation (e.g. Pipanaco basin, Fig. 12). It is important to note that, in contrast to the southern Puna and the Eastern Cordillera of NW Argentina (Kraemer *et al.*, 1999; Hongn *et al.*, 2007), no Paleogene deformation/sedimentation has been reported in the Sierras Pampeanas.

The Neogene accumulation would have been associated, to the west, with loading by the basement thrust system of the Famatina belt (Dávila & Astini, 2007; Carrapa *et al.*, 2010; Davila, 2010). However, given that the tectonic shortening along the Famatina and related ranges is low (<20%; Dávila, 2003), whereas the depocenters are thick and extend several hundred kilometres away from the topographic loads, Dávila *et al.* (2005, 2007, 2010) concluded that sublithospheric forces might have accompanied the flexural subsidence to accommodate the entire sedimentary filling. To synthesize, the Neogene was essentially a stage of short- and long-wavelength subsidence.

After a major episode of deformation in the Pliocene, which rotated and exhumed the Neogene strata (Figs 1 and 2), Quaternary conglomerates and mudflow deposits accumulated along the Ambato range (Fig. 6) and nearby regions, constituting intermontane and closed-drainage basins. Our interpretation implies that *ca.* 1 km of Quaternary strata would have accumulated along the eastern margin of the Pipanaco basin, assuming the Neogene stratigraphic thickness was relatively constant across the northern Sierras Pampeanas. Although the accommodation space for this accumulation might have been generated by different mechanisms (compaction, thrusting, flexural subsidence and/or forced aggradation within an endorheic basin), flexural isostasy seems to be the most viable explanation (see below).

The subsurface basement thrusts along the western side of the basin (Fig. 11), deduced from gravity deconvolutions (Figs 10 and 11), are probably the main cause of uplift along the western border of the Pipanaco depocenter (Fig. 12). Regionally, this thrust system can be correlated to the east-verging thrust front of the Velasco range to the S (see also Alvarado & Ramos, 2011), and the fault systems of the Capillitas and Belen ranges to the N (Fig. 1). Such a thrust system would also explain the development of syntectonic and progressive unconfomities along the SW border of the basin (Bossi *et al.*, 2009). It is important to note that the coarse conglomerates of the Las Cumbres Formation (and correlatives) would have been deposited during this tectonic episode (Bossi & Muruaga, 2009; Bossi *et al.*, 2009). This basement deformation correlates chronologically with the apatite fission-track cooling ages between ca. 7.6 and 3 Ma recorded at the southern flank of the Capillitas ranges, along the northern margin of the Pipanaco basin (Coughlin, 2000).

Although the local relief and sedimentary accommodation space in the Pipanaco basin can be associated with basement thrusting (see above), the long-wavelength (>300 km) and high-elevation of the northern Sierras Pampeanas depocenters (Fig. 4) require an alternative explanation (see also Dávila *et al.*, 2005). Note that the major topographic change is not located at the southernmost Andean plateau boundary, as has been largely stated in the literature, but rather in the Sierras Pampeanas broken foreland (Fig. 4).

In the Sierras Pampeanas, the main basement thrusting event occurred between *ca.* 5 and 3 Ma (Strecker *et al.*, 2009). The amount of shortening associated with this deformation, estimated at different latitudes and across different ranges (e.g. Jordan & Allmendinger, 1986; Kley *et al.*, 1999; Hilley & Coutand, 2010), seems insufficient to explain the strong variation in large-scale topography (see Dávila *et al.*, 2005) or to explain the changes in crustal thickness (Mcglashan *et al.*, 2008; Fig. 4). Some recent studies have proposed that high-elevation basins could have been generated by sedimentary filling (forced aggradation) of closed-drainage and intermontane basins dominated by arid climates (e.g. Sobel *et al.*, 2003), which favour the preservation of thousands of metres of alluvial deposits. However, the sedimentary thicknesses extrapolated along strike (i.e. N–S) in the Sierras Pampeanas do not show significant variation (Fig. 4) to support a regional high-elevated surface controlled by sediment aggradation. The northernmost Sierras Pampeanas is higher in altitude, but preserves less or approximately the same amount of sediments with respect to the southern part (Fig. 4). It is difficult to find a clear correlation between the geometry of the basins along strike, sediment source area and the aggradation-controlled basin elevation (see W–E swaths in Fig. 5). For example, the Rioja Basin is smaller than Pipanaco; however, the accumulation is similar in both depocenters. Our flexural analysis reproduces the space to accommodate the stratal thicknesses recorded across strike. Recently, Strecker *et al.* (2009) also discarded the aggradation hypothesis for the formation of high-elevation basins based on diachronous sediment accumulation along and across strike, as well as on the degree of compensation of the topography, which implies that the long-wavelength signal of the landscape is more plausibly explained by geodynamic processes.

The topographic changes along strike can also be analysed by correlating the surface and subsurface topographies. The top of basement below the intermontane basins shows a remarkable step of *ca.* 5700 m between the northern and southern Sierras Pampeanas. This step

correlates with the position of a *ca.* 2-km step in the surface topography (see Figs 4, 5 and 12) recorded along strike in the regional swath profile. Notice that errors associated with the gravity inversions are ±800 m and therefore do not greatly influence the magnitude of this step (Fig. 4 and Appendix). The removal of the sediment load by a flexural correction (using a loading width of 50 km, a sediment column height of 3 km in the Pipanaco basin and 2 km in Campo de Arenal and a density *ca.* 2.4 g/cm^3) decreases the depth to the top of basement between the Campo del Arenal and Pipanaco basins by *ca.* 260 m. The positive correlation between the basement depth and the regional topography appears to be more than a coincidence.

Several lines of evidence (e.g. thermochronology) suggest that uplift was accompanied by strong exhumation along the northern Sierras Pampeanas, comparable in magnitude to the uplift, which occurred in the Puna plateau during the Late Miocene (Carrapa *et al.*, 2006). Accepting our correlation of the dense subsurface bodies (igneous intrusions detected by gravity filtering) with the volcanic complex exposed in the sierra de Belén (Farallón Negro), as well as with others exposed in the Zapata range further west (see Fig. 12), a minimum exhumation of ca.7.5 km would be expected since the Late Miocene along the northern margin of the Pipanaco basin. This estimation is supported by low-temperature thermochronology and burial studies (Coughlin, 2000; Collo *et al.*, 2011), which yields Miocene cooling ages of <8 Ma (the youngest record in the Sierras Pampeanas), preserved under very low geotherms <17°C/km (Collo *et al.*, 2011). Such thermal conditions would require 5–7 km of exhumation to exhume rocks from below the apatite fission-track closure temperature (between 120°C and 90°C, Reiners *et al.*, 2005).

If the long-wavelength topography is compared with regional gravity data (Fig. 4), several interesting features can be observed. The less negative values of Bouguer and isostatic anomalies to the south can be associated with the gradual reduction of the topographic load, as evidenced by the overall reduction of altitude in that direction. However, there is little change in Moho depths (from 49 km to 46 km, Whitman *et al.*, 1996; Mcglashan *et al.*, 2008; Fig. 4). This crustal thickness variation can only explain *ca.* 0.5 km of topography differences (using the simple buoyancy equation). However, the recorded topographic changes are larger. As suggested by seismic wave attenuation studies (Whitman *et al.*, 1996) and magnetotelluric soundings (Febrer *et al.*, 1982), the negative gravity anomalies could be related to the presence of a shallow asthenosphere below the northern Sierras Pampeanas and Puna. Thus, the higher elevation might be related to isostatic uplift driven by a thinner, lighter and more buoyant lithosphere.

The simplest explanation would be that the northern Sierras Pampeanas is a transitional zone towards the high Andean plateau (see Fig. 4). This zone matches with an offset between the seismic and isostatic Mohos (Fig. 4) (e.g. Whitman *et al.*, 1996), which is consistent with compensation levels below the crust (lower lithosphere or asthenosphere). The Puna plateau topography has been related to lithospheric that would also drive volcanic activity (Kay *et al.*, 1994). Thus, an alternative explanation supposes that these lithospheric removal deep-seated processes (delamination, dynamic topography, etc.) shifted to the south, embracing the closed-drainage basins along the northern Argentine broken foreland. This would have triggered the rise of the intermontane basins to generate the plateau-like morphology, similar to the Altiplano-Puna (Garzione *et al.*, 2008). This interpretation is also consistent with magnetotelluric studies, which interpreted a thermal anomaly and mantle attenuation along this transitional zone of NW Argentina (Febrer *et al.*, 1982). However, it is important to highlight that the Sierras Pampeanas lack a volcanic signature younger than the Late Miocene (Kay & Mpodozis, 2002).

Two end-member hypotheses for the rising of the Andean plateau are: (1) a rapid rise of *ca.* 2.5 km that occurred between 10 and 6 Ma (Garzione *et al.*, 2008) and (2) a slow and steady rise since *ca.* 40 Ma (Barnes & Ehlers, 2009). The filling and uplift history in the Pipanaco basin is Mio-Pliocene or later. This inference, together with the lack of Paleogene sedimentation along and across strike, discredits the idea of a slow and steady rising mechanism at least for the southern margin of the high Andean plateau. In fact, there is not even any Early Miocene sedimentation in the Pipanaco basin and surrounding regions to support uplift of the Puna Plateau prior to *ca.* 12–10 Ma.

CONCLUSION

The Pipanaco basin experienced two major filling stages during the Miocene and the late Pleistocene, separated by basement deformation, which would have occurred in the Plio-Pleistocene. The basin geometry was interpreted using stratigraphic correlations of outcrops and gravity inversions. Although the *ca.* 2 km thick Neogene deposits are probably related to long-wavelength foreland subsidence associated with loads located to the west (High Andes and Famatina) complemented by dynamic forces (e.g. Dávila *et al.*, 2010), the Quaternary would have been deposited within intermontane and closed-drainage basin, driven by local topographic loads (similar to the Present-day Sierras Pampeanas ranges). Approximately 1 km of Quaternary strata were interpreted from gravity analysis along the eastern part of the Pipanaco basin (assuming that Neogene deposits are distributed homogenously along this part of the northern Sierras Pampeanas), a thickness that can be entirely reproduced by topographic loading of the Ambato range, located to the East.

No clear relationship between sediment filling and surface topography could be deduced along strike between the Andean plateau and the Sierras Pampeanas.

Accumulation in the Pipanaco basin was more substantial than in other regions within the southern Andean plateau, but the mean altitude of the basin is lower. The incorporation of the broken foreland into the plateau belt and the high-elevated basins in the Sierras Pampeanas does not seem to have been produced by sediment aggradation within closed-drainage depocenters (e.g. Sobel *et al.*, 2003). The good correlation between surface topography and depth to basement suggests that differential surface uplift from S to N might be the main cause of the long-wavelength topography in this part of the Andes. As crustal thickness variations are limited, such surface uplift is interpreted to result from deeper lithospheric processes. This conclusion is consistent with the Strecker *et al.* (2009) model, which shows that the northern Sierras Pampeanas topography was controlled by deep-seated geodynamics. These mechanisms produced a buoyant lithosphere to the North, which would be responsible for the observed uplift.

APPENDIX

GRAVITY DATA COLLECTION

Figure A1 shows the distribution of altimetry/gravity measurements. A single-frequency topographic GPS (Global Positioning System) was used to obtain reliable positioning for all measurements, with a 0.3 m error in each location. The altitude data for each station was obtained from a digital elevation model from the Shuttle Radar Topography Mission (SRTM, NASA) (Fig. A1).

A Scintrex CG-3 Autograv Gravity Meter was used in the gravity survey, which consists of a number of daily loops, and begin and end with readings at the same point (the drift base), where consequently the drifts can be monitored. To reduce the relative error of the gravity anomaly to 5%, three measurements were taken per base with an accuracy of 0.05 mgal.

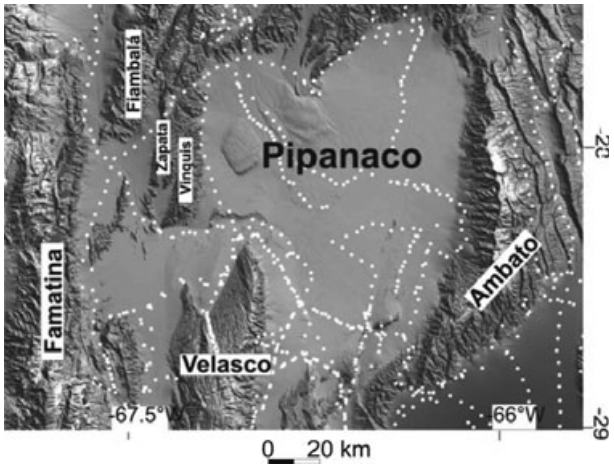

Fig. A1. Distribution (white points) of the gravity survey along the Pipanaco basin.

GRAVITY CORRECTION

Calculation of gravity anomalies

The gravity anomalies were calculated using (Blakely, 1995):

$$\mathrm{FAA} = \mathrm{g_o} - (\gamma \mathrm{o} - \mathrm{FAC}) \qquad (A1)$$

$$\mathrm{BA} = \mathrm{g_o} - (\gamma o - \mathrm{FAC} + \mathrm{BC} + \mathrm{TC}) \qquad (A2)$$

Where FAA is the Free-air anomaly (mGal), BA is the Bouguer anomaly (mGal); g_o is the observed gravity (mGal) and γo is the theoretical gravity, in the Geodetic Reference System (1971); FAC is the free-air correction (mGal); BC is Bouguer correction (mGal); TC is the topographic correction (mGal), and masses up to a distance of about 167 km (Hayford zone O2) are considered. These corrections are calculated as:

$$\mathrm{FAC} = \partial \mathrm{g}/\partial \mathrm{z} \qquad (A3)$$

$$\mathrm{BC} = (2\pi \mathrm{G}\rho_c)\mathrm{h} \qquad (4)$$

G is the gravitational constant (6.672×10^{-11} m^3 kg^{-1} s^{-2} or 6.672×10^{-6} m^2 kg^{-1} mGal); ρ_c is the density of crustal rock (kg m^{-3}); h is the elevation above mean sea level (m); and $\partial g/\partial z$ is the vertical gradient of gravity.

A vertical gradient of 0.3086 mGal/m for the free-air correction and a density of 2.67 g/cm^3 were used to calculate the Bouguer correction (Hinze, 2003).

These data, together with additional information from the Geofísico Sismológico Volponi Institute (San Juan, Argentina) and the Física Institute (Rosario, Argentina), was used to construct a regionally corrected Bouguer anomaly map. The measured values were normalized by the minimum curvature technique in a regular grid of 5×5 km.

Separation of gravity anomalies

Given that the Bouguer anomaly map (Fig. A2 and Fig. 4 in the article) shows a long-wavelength (>200 km) negative gradient and that gravity data stack the influence of a different scale gravity effect, we separated the short-wavelength gravity anomaly along the regional transect for a better visualization of the structure and composition in the studied region (see Fig. 7 in the manuscript).

A signal-processing filter was used to create as flat a frequency response as possible in the passband. Among the different filters (see Blakely, 1995; Torge, 2001), the Butterworth filter was selected (a maximally flat magnitude filter) in a 250-km window of order 8 (Blakely, 1995), as it was the most efficient in previous analysis of the Andean crustal root (see Introcaso, 1999; Götze & Krause, 2002) to discern between short-wavelength anomalies.

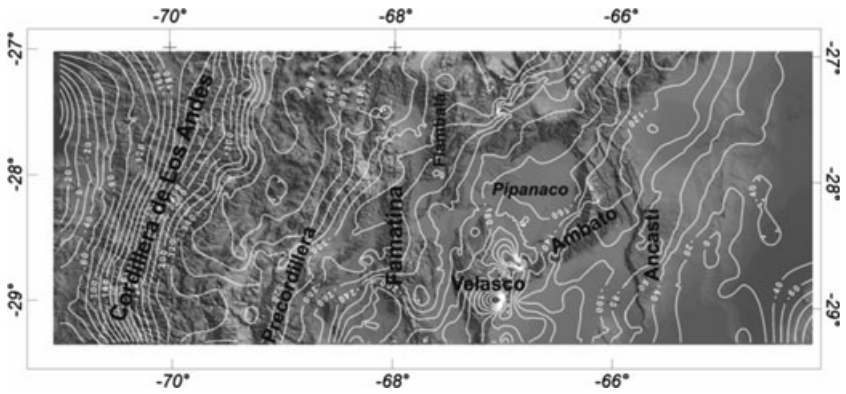

Fig. A2. Regional Bouguer anomaly map between 27º and 29º SL, from the High Andes to the Argentine broken foreland.

Three-dimensional gravity inversion model

We used the GMSYS-3D program (Popowski *et al.*, 2006) to calculate the depth of two layers with known densities. The layer densities were calculated from the average velocities from seismic refraction tests conducted by YPF in 1982 in the southern Pipanaco and La Rioja basins. For the conversion from wave velocities into density, the Brocher (2005) approach was used, which allowed us to estimate an average density for the sedimentary fill as 2.37 g/cm^3 and for the basement, 2.70 g/cm^3. With this model, the subsurface limits of the basement top can be set, and the geometry of the sedimentary units can be constrained.

Spectral analysis

Power spectrum analysis has been widely used in previous works to interpret gravity anomalies (Spector & Grant, 1970; Gerard & Debeglia, 1975; Bhattacharyya, 1978; Dimri, 1992; Blakely, 1995). The logarithm of the radial average of the energy spectrum (the square of the Fourier amplitude spectrum) is plotted against the radial frequency. The slopes of the linear segments of the spectrum correspond to separate depth ensembles and provide the parameters, which are used for the design of numerous filters. The slope of each segment provides information about the depth to the top of an ensemble of magnetic or gravity bodies (for more details see Kivior & Boyd, 1998).

This analysis, however, provides limited information about the geometry of the sources. All values are calculated for point-shaped sources (spheres) and thus are maximum source depths, due to the principle of equivalence in the wave number domain. The depth to the source bodies is related to the slope of the logarithm of the power spectrum as a function of the logarithm of the wave number. These depths represent statistical estimates of the interfaces, which allow for an evaluation of an average structural model (Lim & Malik, 1981; Guspí & Introcaso, 2000).

The location where the average depths were evaluated is listed as B and C in Fig. 8 (in the manuscript). Circle B shows the depths of the sedimentary units, whereas C represents the average depth of the anomalous density bodies. Figure 8a (in the manuscript) shows the average radial power spectrum and Fig. 9b (in the manuscript) the estimated depth. The maximum depth of the sedimentary units is ca.2500–3000 metres (see Fig 9b in the manuscript), which confirms the 3D basement-top model. The average depth to the roof of the anomalous density bodies is ca.5000 metres.

Euler deconvolution

This technique provides estimates of the source location and depth. Therefore, Euler deconvolution is both a boundary finder and depth estimator. Conventional Euler deconvolution (Reid *et al.*, 1990) estimates the spatial position and shape type of sources by assuming interpretation models of one singular point (Stavrev & Reid, 2010). One-point sources have their position described by a single spatial location, e.g. the sphere centre, the thin rod top or sheet edge, the axis of an infinite circular cylinder or the infinite contact top corner. The source coordinates and the shape index, known as "structural index (N) (after Thompson, 1982), are coefficients in Euler's differential equation for homogeneous functions of degree $n = -N$. This equation enables practical inversions of massive data sets. The most useful results of Euler deconvolution are the delineation of trends and depths. The Euler deconvolution method (Thompson, 1982; Reid *et al.*, 1990; Keating, 1998; Zhang *et al.*, 2000; Stavrev & Reid, 2010) tracks anomalous gravity gradients on profiles or maps. Thompson (1982) based this technique upon Euler's homogeneity equation, whereas Reid *et al.* (1990) developed the 3-D forms of Euler's equation to analyse magnetic data. The obtained gradients are usually associated with a density variation due to, for example intrusions, tectonic structures, facies changes, etc. The solutions are a set of points (usually x, y, z) that also estimate the depth of the geological structures which cause the gravity anomalies. This method requires an understanding of a critical parameter, the structural index S1, which characterizes the source geometry. In gravity, this index is 0.5 and 2 (Reid *et al.*, 1990; Keating, 1998; Barbosa *et al.*, 1999; Roy *et al.*, 2000; Silva *et al.*, 2001). The 3-D form of the Euler's

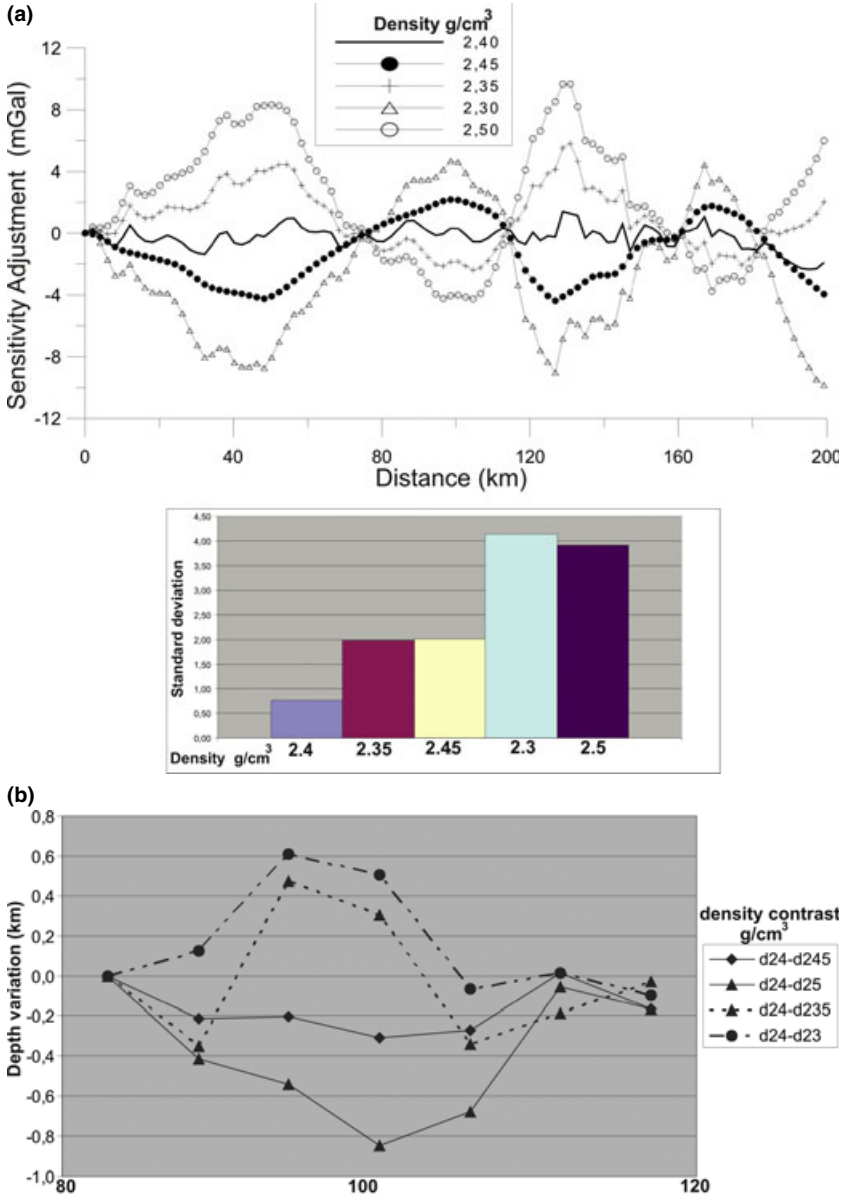

Fig. A3. (a) Sensitivity of the gravimetric effect of the model by varying the density contrast between the sedimentary and basement. (b) Variation in the depth of basin caused by variations in the density contrast between sediments and basement.

equation is easily applied to gridded data using a mobile square window.

To determine the geometry of the anomalous bodies and to get an idea of the three-dimensional form, an analytical signal was calculated (see below).

Analytic signal

This technique, known also as the total gradient method, is based on the methodology developed by Nabiaghian (1972, 1974)), which applies the concept of an analytic signal to the potential field data in 2D. This enhances the gravity anomalies produced by geologic discontinuities of medium to short wave, revealing the edges of anomalous bodies (Nabiaghian, 1972). Nabiaghian (1984), Roest *et al.* (1992) and Salem & Smith (2005) developed this method in 3D.

The absolute value of the analytic signal is defined as follows:

$$|A(x,y)| = \sqrt{\left(\frac{\partial}{\partial x F(x,y)}\right)^2 + \left(\frac{\partial}{\partial y F(x,y)}\right)^2 + \left(\frac{\partial}{\partial z F(x,y)}\right)^2} \quad (A5)$$

Where $|A\ (x,y)|$ is the analytical signal modulus, $F\ (x,y)$ is the gravity field and $\frac{\partial}{\partial x}F(x,y)$; $\frac{\partial}{\partial y}F(x,y)$; $\frac{\partial}{\partial z}F(x,y)$ are directional derivates.

Our results show that the high-density masses are not projected in map view as bands, compatible with deeper and higher density basement blocks raised by tectonics. In contrast, they have circular to elliptical shapes, which suggest high-density body intrusions, at least higher in density than the country rock (granodiorites).

Two-dimensional gravity model

An E-W 2D gravity profile is depicted in Fig. 11 (A–A′, in the manuscript) that was obtained using the software pack developed by the Northwest Geophysical Associates, Inc. (Webring, 1985). This model requires the aid of additional data to constrain the observed and modelled profile. We used the stratigraphy, as well as the geological and geophysical data described previously.

Errors associated to depth estimations

If the estimated mean density of the sedimentary cover of *ca.* 2.4 g/cm^3 is considered a representative value, then a sensitivity adjustment analysis allows for an estimation of the maximum difference in the basin depth estimation. Figure A3 shows a maximum *ca.* 800 m depth difference by changing densities ±0.1 g/cm^3.

BASIN AND TOPOGRAPHIC ANALYSIS

Backstripping

A 1D Airy backstripping programme developed by Cardozo (OSXBackstrip) was run to discern the influences of the sedimentary loading and differential compaction across the Pipanaco basin. This compaction-driven subsidence analysis is based on the exponential reduction of porosity, which creates accommodation space (cf. Allen & Allen, 1990). Stratigraphic and sedimentological data were supplied from the stratigraphic and sedimentological information provided above and from previous work in the region and nearby regions. We used the petrophysical properties (porosity and grain densities) proposed by Allen & Allen (1990).

Flexural model

The crustal bending of the Pipanaco basin was computed using the 2D formulation of Cardozo & Jordan (2001) and the 2D flexural model developed by Cardozo (OSXFlex2D). The density of the loads is ∂_{load} = 2700 kg/m^3, given that the region is dominated by basement thrusts (granitoids and gneises). This model assumes flexural compensation with respect to the mantle (∂_m = 3300 kg/m^3). A mean effective elastic thickness (Te) of 40 km was used, consistent with recent geophysical approaches (Tassara, 2005; Pérez Gussinyé *et al.*, 2007; Tassara *et al.*, 2007). The influence of the compressive stress on distal foreland lithosphere was not evaluated because GPS intraplate velocity studies have demonstrated insignificant displacement in the easternmost areas of the Sierras Pampeanas (Brooks *et al.*, 2003).

Given that the Late Miocene strata along and across the region suggest that the Pipanaco basin and its nearby ranges were depositional areas, it can be assumed that the shortening and the modern topographic area (volume) of the Sierras de Ambato (load, see Fig. 13 in the article) represents the tectonic load that affected the eastern margin of the basin. The topographic loading profile (Ambato range) was built as discrete rectangles of ca. 5 km in width, whereas the height of the rectangles correspond to the modern topography, plus an extra area required to fit the modelled topography with the observed topography.

Morphotectonic profiles

To analyse the topography in the southern border of the Andean plateau, between the Puna and the Sierras Pampeanas, we first need to reduce the 'noise' generated by sedimentation and to track the position of the basin floor with respect to the modern mountain system.

Four N–S swath profiles were constructed (see Fig. 4 in the article): (1) mean, maximum and minimum topographies, (2) relief or differential topography (the difference between the highest and lowest topography), (3) sedimentary accumulation profiles and (4) a profile to the basement top. Profiles (1) and (2) were conducted using DEM (SRTM 90 m), whereas (3) and (4) required the analysis of geological and geophysical information (seismic lines and gravity profiles). For the regions located in the north and south (Campo del Arenal and La Rioja), the interpretation of seismic sections was used (Cristallini *et al.*, 2004; Mortimer *et al.*, 2007; Bossi & Muruaga, 2009). In the Pipanaco basin, the 2D gravity model generated in this work was applied. It is important to note that the sedimentary thicknesses inferred from the seismic data in La Rioja was contrasted with gravity (Gimenez *et al.*, 2009) to reduce the uncertainties in the Pipanaco depocenter thickness estimations, where seismic sections are not available. Three W-E swaths (Fig. 5 at 27°, 28°, and 29° SL) depicting minimum, maximum and relief were constructed to support the N-S swaths.

ACKNOWLEDGEMENTS

FONCyT, CONICET, SECyT support our work in the Argentine Broken Foreland. We appreciate discussions and comments from colleges from the Centro de Análisis de Cuencas, Universidad Nacional de Córdoba and Universidad Nacional de San Juan. FMD thanks the Royal Society (UK) and the Marie Curie Fellowship IIF Program (ANDYN project) for supporting his studies. We appreciate the suggestions of P. van der Beek (Editor) and comments and corrections from reviewers Teresa Jordan, Victor Ramos and George Hilley, which significantly improved our work.

REFERENCES

Allen, P.A. & Allen, J.R. (1990) *Basin Analysis: Principles and Applications*. 2nd edn, Blackwell Publishing, Oxford, UK, pp. 549. 2005. ISBN 0-632-05207-4.

Allmendinger, R.W., Jordan, T.E., Kay, S.M. & Isacks, B.L. (1997) The evolution of the Altiplano-Puna Plateau of the Central Andes. *Annu. Rev. Earth Planet Sci.*, **25**, 139–174.

Alvarado, P. & Ramos, V.A. (2011) Earthquake deformation in the northwestern Sierras Pampeanas of Argentina based on seismic waveform modeling. *J. Geodynamics*, **51**, 205–218.

Astini, R.A. (2009) El marco tectónico de la glaciación carbonífera. XII Congreso Geológico Chileno, Extended Abstracts: S10–003:1-4. 22–26., Santiago de Chile, Chile, Servicio Nacional de Geologia y Mineria, Chile.

Bain, N. (2001) Petrological and geochemical contribution to the Farallón Negro Volcanic Complex, NW-Argentina. Diploma thesis, Swiss Federal Institute of Technology, Zurich, 92 pp.

Barbosa, V.C.F., Silva, J.B.C. & Medeiros, W.E. (1999) Stability analysis and improvement of structural index estimation in Euler deconvolution. *Geophysics*, **64**, 48–60.

Barnes, J.B. & Ehlers, T.A. (2009) End member models for Andean Plateau uplift. *Earth Sci. Rev.*, **97**, 117–144.

Bhattacharyya, B.K. (1978) Computer modeling in gravity and magnetic interpretation. *Geophysics*, **43** (5), 912–929.

Blakely, R.J. (1995) *Potential Theory in Gravity and Magnetic Applications*. Cambridge University Press, Cambridge, UK, 441 pp.

Bossi, G.E. & Muruaga, C.M. (2009) Estratigrafía e inversión tectónica del "rift" neógeno en el Campo del Arenal, Catamarca, NO Argentina. *Andean Geol.*, **36** (2), 311–341.

Bossi, G.E. & Palma, R. (1982) Reconsideración de la estratigrafía del Valle de Santa María, Provincia de Catamarca, Argentina. *Congreso Latinoamericano de Geología 5*, Proceeding **1**, 155–172, Buenos Aires.

Bossi, G.E., Muruaga, C., Georgieff, S., Ahumada, A.L., Ibáñez, L. & Vides, M.E. (1997) The Santa María Neogene Basin of the Pampean Ranges: an example of mixed tectonic evolution. *Congreso Latinoamericano de Sedimentología, 1, Sociedad Venezolana de Geólogos*, **1**, 97–104. Caracas.

Bossi, G.E., Muruaga, C. & Gavriloff, I.J.C. (1999) Ciclo Andino. Neógeno-Pleistoceno. Sedimentación. In: *14th Congreso Geológico Argentino Relatorio 1* (Ed. by G. González Bonorino, R. Omarini & J. Viramonte), pp. 329–360. Salta, Argentina.

Bossi, G.E., Georgieff, S.M. & Gavriloff, I.J.C. (2000) Tectosedimentary regional scheme of the Neogene basins of the Pampean Ranges, Argentina. II Congreso Latinoamericano de Sedimentología and VII Reunión Argentina de Sedimentología, Abstracts, 52. Asociacion Argentina de Sedimentologia, Mar del Plata, Argentina.

Bossi, G.E., Georgieff, S.M. & Vides, M.E. (2007) Arquitectura y paleoambientes de los depósitos fluviales gravosos de la Formación Las Cumbres (Neógeno), en Villa Mervil, La Rioja, Argentina. *Lat. Am. J. Sedimentol. Basin Anal.*, **14** (1), 53–57.

Bossi, G.E., Georgieff, S.M., Muruaga, C.M., Ibáñez, L.M. & Sanagua, J.G. (2009) Los conglomerados sintectónicos de la Formación Las Cumbres (Plio-Pleistoceno), Sierras Pampeanas de La Rioja y Catamarca, Argentina. *Andean Geol.*, **36** (2), 172–196.

Brocher, T.M. (2005) Empirical relations between elastic wavespeeds and density in the earth's crust. *Bull. Seismological Soc. Am.*, **95** (6), 2081–2092.

Brooks, B.A., Bevis, M., Smalley, R.K., Kendrick, E., Manceda, R., Lauría, E., Maturana, R. & Araujo, M. (2003) Crustal motion in the Southern Andes (26°–36°): do the Andes behave like a microplate. *Geochem. Geophys. Geosyst.*, **4**, 1085.

Butler, R.F., Marshall, L.G., Drake, R.E. & Curtis, G.H. (1984) Magnetic polarity stratigraphy and 40K-40Ar dating of late Miocene and early Pliocene continental deposits, Catamarca province, NW Argentina. *J. Geol.*, **92**, 623–636.

Büttner, S.H. (2009) The Ordovician Sierras Pampeanas – Puna basin connection: basement thinning and basin formation in the Proto-Andean back-arc. *Tectonophysics*, **477**, 278–291.

Caelles, J.C., Clark, A.H., Farrar, E., Mcbride, S.L. & Quirt, S. (1971) Potassium-argon ages of porphyry copper deposits and associated rocks in the Farallón Negro-Capillitas district, Catamarca, Argentina. *Econ. Geol.*, **66**, 961–964.

Caminos, R. (1979) Sierras Pampeanas Noroccidentales Salta, Tucumán, Catamarca, La Rioja y San Juan. In: *Segundo simposio de Geología Regional Argentina 1* (Ed. by J.C. Turner), pp. 225–291, Academia nacional de ciencias, Córdoba.

Cardozo, N. & Jordan, T.E. (2001) Causes of spatially variable tectonic subsidence in the Miocene Bermejo foreland basin, Argentina. *Basin Res.*, **13**, 335–357.

Carrapa, B., Sobel, E.R. & Strecker, M.R. (2006) Orogenic Plateau growth in the Central Andes: evidence from sedimentary rock provenance and apatite fission track thermochronology in the Fiambala Basin, southernmost Puna Plateau margin (NW Argentina). *Earth Planet. Sci. Lett.*, **247**, 82–100.

Carrapa, B., Hauer, J., Schoenbohm, L., Strecker, M.R., Schmitt, A.K., Villanueva, A. & Sosa Gomez, J. (2008) Dynamics of deformation and sedimentation in the northern Sierras Pampeanas: an integrated study of the Neogene Fiambalá basin, NW Argentina. *Geol. Soc. Am. Bull.*, **120** (11/12), 1518–1543.

Carrapa, B., Hauer, J., Schoenbohm, L., Strecker, M.R., Schmitt, A.K., Villanueva, A. & Sosa Gómez, J. (2010) Dynamics of deformation and sedimentation in the northern Sierras Pampeanas: an integrated study of the Neogene Fiambala Basin, NW Argentina: comment and discussion. *Geol. Soc. Am. Bull.*, **122**, 950–953.

Collo, G., Dávila, F.M., Nóbile, J.C., Astini, R.A. & Gehrels, G. (2011) Burial and thermal history of the Vinchina foreland basin, W Argentina (28°–29°SL): signature of the Neogene flat subduction in the Andes? *Tectonics*, **30**, TC4012, doi:10.1029/2010TC002841.

Coughlin, T.J. (2000) Linked orogen-oblique fault zones in the Central Andes: implications for Andean orogenesis and metallogenesis. Unpublished PhD Thesis, University of Queensland, Queensland.

Cristallini, E.O., Comínguez, A.H., Ramos, V.A. & Mercerat, E.D. (2004) Basement double-wedge thrusting in the northern Sierras Pampeanas of Argentina Constraints from deep seismic reflection. In: *Thrust Tectonics and Hydrocarbon Systems* (Ed. by K.R. McClay) Am. Assoc. Petrol. Geol. Mem., **82**, 65–90.

Dahlquist, J., Pankhurst, R., Rapela, C., Casquet, C., Fanning, C., Alasino, P. & Baez, M. (2006) The San Blas Pluton: an example of Carboniferous plutonism in the Sierras Pampeanas, Argentina. *J. South Am. Earth Sci.*, **20**, 341–350.

Davila, F.M. (2010) Dynamics of deformation and sedimentation in the northern Sierras Pampeanas: an integrated study of the Neogene Fiambala Basin, NW Argentina: comment and discussion. *Geol. Soc. Am. Bull.*, **122**, 946–949.

Dávila, F.M. (2003) Transecta estratigráfica-estructural a los 28°30′–28°54′ de Latitud Sur, sierra de Famatina, provincia de La Rioja, República Argentina. Unpublished PhD Thesis, Facultad de Ciencias Exactas, Físicas y Naturales, Universidad Nacional de Córdoba, Argentina.

Dávila, F.M. & Astini, R.A. (2003) Early Middle Miocene broken foreland development in the southern Central Andes: evidence for extension prior to regional shortening. *Basin Res.*, **15**, 379–396.

Dávila, F.M. & Astini, R.A. (2007) Cenozoic provenance history of synorogenic conglomerates in western Argentina (Famatina Belt): implications for Central Andean foreland development. *Geol. Soc. Am. Bull.*, **119**, 609–622.

Dávila, F.M., Astini, R.A., Jordan, T.E. & Kay, S.M. (2004) Early Miocene andesite conglomerates in the Sierra de Famatina, broken foreland region of western Argentina, and documentation of magmatic broadening in the south-central Andes. *J. South Am. Earth Sci*, **17**, 89–101.

Dávila, F.M., Astini, R.A. & Jordan, T.E. (2005) Cargas subcorticales en el Antepaís Andino y la planicie pampeana: evidencias estratigráficas, topográficas y geofísicas. *Rev. Asoc. Geol. Argent.*, **60** (4), 775–786.

Dávila, F.M., Astini, R.A., Jordan, T.E., Gehrels, G. & Ezpeleta, M. (2007) Miocene forebulge development previous to the broken foreland partitioning in the southern Central Andes, west-central Argentina. *Tectonics*, **26**, TC5016.

Dávila, F.M., Lithgow-Bertelloni, C. & Giménez, M. (2010) Tectonic and dynamic controls on the topography and subsidence of the Argentine Pampas: the role of the flat slab. *Earth Planet. Sci. Lett.*, **295** (1–2), 187–194.

Decelles, P.G. & Giles, K.A. (1996) Foreland basin systems. *Basin Res.*, **8**, 105–123.

Dimri, V.P. (1992) *Deconvolution and Inverse Theory*. Elsevier Science Publishers, Amsterdam, London, New York, Tokyo.

Duarte, R.G. (1997) Gliptodontes del pleistoceno tardío de Agua de las Palomas, Campo del Pucara, Catamarca, Argentina. Variaciones morfológicas del caparazón de Glyptodon Reticulatus Owen, 1845. *Ameghiniana*, **34** (3), 345–355.

Eremchuck, J.E. (1984) Fracturas del Borde Occidental de las Sierras de Ambato-Manchao, Provincia de Catamarca. *IX Congreso Geológico Argentino*, **II**, 362–367. Bariloche.

Ezpeleta, M., Dávila, F.M. & Astini, R.A. (2006) Estratigrafía y paleoambientes de la Formación Los Llanos (La Rioja, Argentina): Una secuencia condensada miocena en el antepaís fragmentado andino central. *Revista de la Asociación Geológica Argentina*, **61**, 171–186.

Febrer, J., Baldis, B., Gascón, J., Mamani, M. & Pomposiello, C. (1982) La anomalía geotérmica Calchaquí en el noroeste argentino: Un nuevo proceso geodinámico asociado a la subducción de la placa de Nazca. *Actas del V Congreso Latinoamericano de Geología, Argentina*, **III**, 691–703, Buenos Aires

Fisher, N.D., Jordan, T.E. & Brown, L. (2002) The structural and stratigraphic evolution of the La Rioja basin, Argentina. *J. South Am. Earth Sci.*, **15**, 141–156.

Galván, A. & Ruiz Huidobro, O. (1965) Geología del Valle de Santa María. Estratigrafía de las Formaciones Mezosoico-Terciarias. *Acta Geológica Lilloana*, **7**, 217–230.

Garzione, C.N., Hoke, G.D., Libarkin, J.C., Withers, S., Macfadden, B., Eiler, J., Ghosh, P. & Mulch, A. (2008) Rise of the Andes. *Science*, **320** (5881), 1304.

Gavriloff, I.J.C. & Bossi, G.E. (1992) Revisión general, análisis facial, correlación y edades de las Formaciones San José y Río Salí (Mioceno medio), provincias de Catamarca, Tucumán y Salta, República Argentina. *Acta Geológica Lilloana*, **17** (2), 5–43.

Gerard, A. & Debeglia, N. (1975) Automatic threedimensional modeling for the interpretation of gravity or magnetic anomalies. *Geophysics*, **40** (6), 1014–1034.

Gimenez, M.E., Martinez, M.P., Jordan, T., Ruíz, F. & Lince Klinger, F. (2009) Gravity characterization of the La Rioja Valley Basin, Argentina. *Geophysics*, **74** (3), B83–B94.

González Bonorino, F. (1950) Geología y Petrografía de las Hojas 12d (Capillitas) y 13d (Andalgalá). *Boletín Dirección General de Industria Minera*, **70**, 1–100, Buenos Aires.

González Bonorino, F. (1972) Descripción Geológica de la Hoja 13c Fiambalá, Provincia de Catamarca. Carta Geológico-económica de la República Argentina. *Boletín Dirección Nac. Geol. Min.*, **127**, 1–7.

González Díaz, E.F. (1970) El Carbónico Superior alto (Westfaliano-Estefaniano) de la quebrada de La Cébila (NE de La Rioja). *4ª Jornadas Geológicas Argentinas, Proceedings*, **2**, 163–186, Mendoza.

Götze, H.-J. & Krause, S. (2002) The Central Andean gravity high a relic of an old subduction complex? *J. South Am. Earth Sci.*, **14**, 799–811.

Guspí, F. & Introcaso, B. (2000) A sparse spectrum technique for gridding and separating potential field anomalies. *Geophysics*, **65**, 1154–1161.

Halter, W.E., Bain, N., Becker, K., Heinrich, C.A., Landtwing, M.R., Von Quadt, A., Clark, A.H., Sasso, A.M., Bissig, T. & Tosdal, R.M. (2004) From andesitic volcanism to the formation of a porphyry Cu-Au mineralizing magma chamber: the Farallón Negro Volcanic Complex, northwestern Argentina. *J. Volc. Geoth. Res.*, **136**, 1–30.

Hilley, G.E. & Coutand, I. (2010) Links between topography, erosion, rheological heterogeneity, and deformation in contractional settings: insights from the Central Andes. *Tectonophysics*, **495** (1–2), 78–92.

Hinze, W.J. (2003) Bouguer reduction density: why 2.67? *Geophysics*, **68** (5), 1559–1560.

Hockenreiner, M., Sollner, F. & Millar, H. (2003) Dating the TIPA shear zone: an Early Devonian terrane boundary between the Famatinian and Pampean systems (NW Argentina). *J. South Am. Earth Sci.*, **16**, 45–66.

Hongn, F., Del Papa, C.J., Powel, I.A., Petrinovic Mon, R. & Deraco, V. (2007) Middle Eocene deformation and sedimentation in the Puna-Eastern Cordillera transition (23°–26°S): inheritance of pre-existing heterogeneities on the pattern of initial Andean shortening. *Geology*, **35**, 271–274.

Introcaso, B. (1999) *Algunos elementos para el tratamiento de anomalías de campos potenciales*. Instituto de Física de Rosario, Libro 3, Temas de Geociencia, Rosario, Argentina, 50 pp.

Jordan, T.E. & Allmendinger, R.W. (1986) The Sierras Pampeanas of Argentina: a modern analogue of Rocky Mountain foreland deformation. *Am. J. Sci.*, **286**, 737–764.

Jordan, T.E., Zeitler, P., Ramos, V.A. & Gleadow, A.J.W. (1989) Thermochronometric data on the development of the basement peneplain in the Sierras Pampeanas, Argentina. *J. South Am. Earth Sci.*, **2**, 207–222.

Kay, S.M. & Mpodozis, C. (2002) Magmatism as a probe to the Neogene shallowing of the Nazca plate beneath the modern Chilean flat-slab. *J. South Am. Earth Sci.*, **15**, 39–57.

Kay, S.M., Maksaev, V.A., Moscoso, R., Mpodozis, C., Nasi, C. & Gordillo, C.E. (1988) Tertiary Andean magmatism in Chile and Argentina between 28S and 33S: correlation of magmatic chemistry with changing Benioff zone. *J. South Am. Earth Sci.*, **1**, 21–38.

Kay, S.M., Coira, B. & Viramonte, J. (1994) Young mafic back-ark volcanic rocks as guides to lithospheric delamination beneath the Argentine Puna Plateau, Central Andes. *J. Geophys. Res.*, **99**, 24323–24339.

Keating, P.B. (1998) Weighted Euler deconvolution of gravity data. *Geophysics*, **63**, 1595–1603.

Kivior, I. & Boyd, D. (1998) Interpretation of the aeromagnetic experimental survey in the Eromanga Cooper basin. *Can. J. Explor. Geophys.*, **34**, 58–66.

Kleinert, K. & Strecker, M.R. (2001) Changes in moisture regime and ecology in response to late Cenozoic orographic barriers: the Santa Maria Valley, Argentina. *Geol. Soc. Am. Bull.*, **113**, 728–742.

Kley, J., Monaldi, C.R. & Salfity, J.A. (1999) Along-strike segmentation of the Andean foreland: causes and consequences. *Tectonophysics*, **301**, 75–94.

Kraemer, B., Adelmann, D., Alten, M., Schnur, W., Erpenstein, K., Kiefer, E., Van Den Bogaard, P. & Gorler, K. (1999) Incorporation of the Paleogene foreland into Neogene Puna Plateau: the Salar de Antofalla, NW Argentina. *J. South Am. Earth Sci.*, **12**, 157–182.

Latorre, C., Quade, J. & Mcintosh, W.C. (1997) The expansion of C4 grasses and global change in the table Miocene: stable isotope evidence from the Americas. *Earth Planet. Sci. Lett.*, **146** (1–2), 83–96.

Lim, J.S. & Malik, N.A. (1981) A new algorithm for two-dimensional maximum entropy power spectrum estimation. *IEEE Trans. Acoust. Speech Signal Process.*, **29**, 401–413.

Llambías, E. (1970) Geología de los Yacimientos Mineros de Agua de Dionisio. *Revista de la Asociación Argentina de Mineralogía, Petrología y Sedimentología*, **1** (1–2), 2–32.

Marshall, L.G., Butler, R.F., Drake, R.E., Curtis, G.H. & Tedford, R.H. (1979) Calibration of the great American interchange. *Science*, **204**, 272–279.

Martinez, M.P., Perucca, L.P., Gimenez, M.E. & Ruíz, F. (2008) Manifestaciones geomorfológicas y geofísicas de una estructura geológica profunda al sur de la Sierra de Pie de Palo, Sierras Pampeanas. *Revista de la Asociación Geológica Argentina*, **63** (2), 104–111.

Mcglashan, N., Brown, L. & Kay, S.M. (2008) Crustal thickness in the central Andes from teleseismically recorded depth phase precursors. *Geophys. J. Int.*, **175** (3), 1013–1022.

Mortimer, E.L., Carrapa, B., Coutand, I., Schoenbohm, L., Sobel, E.R., Gomez, J.S. & Strecker, M.R. (2007) Fragmentation of a foreland basin in response to out-of-sequence basement uplifts and structural reactivation: El Cajón–Campo del Arenal basin, NW Argentina. *Geol. Soc. Am. Bull.*, **119** (5/6), 637–653.

Muruaga, C.M. (1998) Estratigrafía y Sedimentología del Terciario Superior de la Sierra de Hualfín, entre las localidades de Villavil y San Fernando, Provincia de Catamarca. PhD Thesis (unpublished), Universidad Nacional de Tucumán, Facultad de Ciencias Naturales e Instituto Miguel Lulo, Tucuman, Argentina.

Muruaga, C.M. (2001a) Estratigrafía del Membro El Jarillal (Formación Chiquimil, Mioceno superior), la Sierra de Hualfín, Catamarca. *Acta Geológica Lilloana*, **18** (2), 265–280.

Muruaga, C.M. (2001b) Estratigrafía y desarrollo tectosedimentario de sedimentos terciarios en los alrededores de la Sierra de Hualfín, borde suroriental de la Puna, Catamarca, Argentina. *Revista de la Asociación Argentina de Sedimentología*, **8** (1), 27–50.

Nabiaghian, M.N. (1972) The analytic signal of two- dimentional magnetic bodies with polygonal cross-secction: its properties and use for automated interpretation. *Geophysics*, **37**, 507–517.

Nabiaghian, M.N. (1974) Aditional comments on the analytic signal of two dimensional magnetic bodies with polygonal cross-section. *Geophysics*, **39**, 85–92.

Nabiaghian, M.N. (1984) Toward a three-dimensional automatic interpretation of potential field data via generalized Hilbert transforms: fundamental relations. *Geophysics*, **49**, 780–786.

Nasif, N.L., Esteban, G. & Georgieff, S.M. (2007) Nuevo registro de vertebrados para la Formación Aconquija, provincia de Catamarca, Noroeste de Argentina. Implicancias cronoestratigráficas y consideraciones paleoambientales. *Acta Geológic Llilloana*, **20** (1), 99–112.

Nóbile, J.C. & Dávila, F.M. (2011) Uplift history of northern Sierras Pampeanas broken foreland, Argentina: a preliminary river profile approach. In: *Actas del XVIII Congreso Geológico Argentino*. Asociacion Geologica Argentina, Neuquén, Argentina.

Penk, W. (1920) Der Südrand der Puna de Atacama (NW Argentinien). Ein Beitrag zur Kenntnis des Andinen Gebirgstypus und der Frage der Gebirgsbildung. *Der Abhandlungen der Sachsischen Akademie der Wissenchaften*, **1**, 3–420, Leipzig.

Pérez Gussinyé, M., Lowry, A.R. & Watts, A.B. (2007) Effective elastic thickness of South America and its implications for intra-continental deformation. *Geochem. Geophys. Geosyst.*, **8**, Q05009.

Popowski, T., Connard, G. & French, R. (2006) *GMSYS-3D: 3D Gravity and Magnetic Modeling for OasisMontaj – User Guide*. Northwest Geophysical Associates, Corvallis, Oregon.

Ramos, V.A., Cristallini, E.O. & Pérez, D.J. (2002) The Pampean fl at-slab of the Central Andes. *J. South Am. Earth Sci.*, **15**, 59–78.

Reid, A.B., Allsop, J.M., Granser, H., Millett, A.J. & Somerton, I.W. (1990) Magnetic interpretation in three dimensions using Euler deconvolution. *Geophysics*, **55**, 80–91.

Reiners, P.W., Ehlers, T.A. & Zeitler, P.K. (2005) Past, present and future of thermochronology. *Rev. Mineral. Geochem.*, **58**, 1–18.

Reynolds, J.H. (1987) Chronology of Neogene Tectonics in Western Argentina (27°–33°S) based on the magnetic polarity stratigraphy of foreland basin sediments. Unpublished PhD Thesis, Dartmouth College, Hanover, USA.

Roest, W.R., Verhoef, J. & Pilkington, M. (1992) Magnetic interpretation using the 3-D analytic signal. *Geophysics*, **57**, 116–125.

Roy, L., Agarwal, B.N.P. & Shaw, R.K. (2000) A new concept in Euler deconvolution of isolated gravity anomalies. *Geophys. Prospect.*, **48**, 559–575.

Salem, A. & Smith, R. (2005) Depth and structural index from normalized local wavenumber of 2D magnetic anomalies. *Geophys. Prospect.*, **53**, 83–89.

Salfity, J.A. & Gorustovich, S. (1983) Paleogeografía de la cuenca del grupo Paganzo (Paleozoico Superior). *Revista de la Asociación Geológica Argentina*, **38**, 437–453.

Sasso, A.M. & Clark, A.H. (1998) The Farallón Negro Group, northwest Argentina: magmatic, hydrothermal and tectonic evolution and implications for Cu-Au metallogeny in the Andean back-arc. *Soc. Econ. Geol. Newsletter*, **34** (1), 8–18.

Silva, J.B.C., Barbosa, V.C.F. & Medeiros, W.E. (2001) Scattering, symmetry, and bias analysis of sourceposition estimates in Euler deconvolution and its practical implications. *Geophysics*, **66**, 1149–1156.

Sobel, E.R. & Strecker, M.R. (2003) Uplift, exhumation and precipitation: tectonic and climatic control of Late Cenozoic landscape evolution in the northern Sierras Pampeanas, Argentina. *Basin Res.*, **15**, 431–451.

Sobel, E.R., Hilley, G.E. & Strecker, M.R. (2003) Formation of internally drained contractional basins by aridity-limited bedrock incision. *J. Geophys. Res.*, **108**(B7), 2344, doi:10.1029/2002JB001883.

Socic, M.V.J. (1972) Descripción Geológica de la Hoja 14d, Tinogasta, Provincias de Catamarca y La Rioja. Carta *Geológico-Económica de la República Argentina*. *Boletín Dirección Nacional de Geología y Minería*. Boletín Nº**129**, 54.

Socic, M.V.J. (1973) Descripción Geológica de la Hoja 14 e, Salar de Pipanaco. Provincias de Catamarca y La Rioja. *Ministerio de Industria y Minería. Subsecretaría de Minería. Servicio Nacional Minero Geológico*. Boletín N **137**, 47 pp.

Spagnuolo, C., Georgieff, S.M. & Rapalini, A.E. (2010) Stratigraphy and first dating of the Las Arcas formation in the Santa Maria Valley, Salta Province, Argentina. 18th International Sedimentological Congress, 821. International Association of Sedimentologists, Mendoza, Argentina.

Spector, A. & Grant, F.S. (1970) Statical models for interpreting aeromagnetic data. *Geophysiccs*, **35**, 239–302.

Stavrev, P. & Reid, A. (2010) Euler deconvolution of gravity anomalies from thick contact/fault structures with extended negative structural index. *Geophysics*, **75**, I51–I58.

Strecker, M.R. (1987) Late Cenozoic Landscape Development, the Santa Maria Valley, Northwest Argentina.Unpublished PhD dissertation, Cornell University, Ithaca, NY, USA, 261 pp.

Strecker, M.R., Bloom, A.L., Carrion, M., Villanueva, A. & Naeser, C. (1984) Piedmont terraces in the Valle de Santa María and in front of southwestern Sierra de Aconquija, provinces of Catamarca, Tucumán and Salta, northwestern Argentina. *IX Congreso Geológico Argentino, Bariloche, Argentina, Actas*, **II**, 448–465.

Strecker, M.R., Cerveny, P., Bloom, A.L. & Malizia, D. (1989) Late Cenozoic tectonism and landscape development in the foreland of the Andes: northern Sierras Pampeanas (26°–28°S), Argentina. *Tectonics*, **8** (3), 517–534.

Strecker, M.R., Alonso, R., Bookhagen, B., Carrapa, B., Coutand, I., Hain, M.P., Hilley, G.E., Mortimer, E., Schoenbohm, L. & Sobel, E.R. (2009) Does the topographic distribution of the central Andean Puna Plateau result from climatic or geodynamic processes? *Geology*, **37**, 643–646.

Tabbutt, K.D. (1986) Fission track chronology of foreland basins in eastern Andes: magmatic and tectonic implications. Unpublished Master Thesis, Dartmouth College, Hanover, USA.

Tassara, A. (2005) Interaction between the Nazca and South American plates and formation of the Altiplano-Puna Plateau: review of a flexural analysis along the Andean margin (15°–34°S). *Tectonophysics*, **399**, 39–57.

Tassara, A., Swain, C., Hackney, R. & Kirby, J. (2007) Elastic thickness structure of South America estimated using wavelets and satellite-derived gravity data. *Earth Planet. Sci. Lett.*, **253**, 17–36.

Tauber, A.A. (2005) Mamíferos fósiles y edad de la Formación Salicas (Mioceno tardío) de la sierra de Velasco, La Rioja, Argentina. *Ameghiniana*, **42**, 443–460.

Tauber, A.A. (2007) Primer yacimiento de huevos de dinosaurios (Cretácico Superior) de la provincia de La Rioja, Argentina. *Ameghiniana*, **44** (1), 11–28.

Thompson, D.T. (1982) EULDPH — A technique for making computer assisted depth estimates from magnetic data. *Geophysics*, **47**, 31–37.

Torge, W. (2001) *Geodesy*. 3rd edn, De Gruyter, Berlín, 416 p.

Tripaldi, A., Net, L., Limarino, C.O., Marenssi, S., Re, G. & Caselli, A. (2001) Paleoambientes sedimentarios y procedencia de la Formación Vinchina, Mioceno, noroeste de la provincia de La Rioja. *Revista de la Asociación Geológica Argentina*, **56**, 443–465.

Tripaldi, A., Reijenstein, H. & Ciccioli, P.L. (2005) Estudio geomorfológico y sedimentológico preliminar del campo eólico de Belén, provincia de Catamarca, Argentina. *XVI Congreso Geológico Argentino*, **3**, 537–544, La Plata.

Vázquez, F. (2010) Geología y estratigrafía neógena en la Quebrada del río Las Lajas (Bolsón de Zapata), Catamarca: Su importancia para entender la evolución tectonoestratigráfica en el antepaís fragmentado. Undergraduate Thesis (unpublished) Universidad Nacional de Córdoba, Argentina.

Verdecchia, S.O., Baldo, E.G., Benedetto, J.L. & Borghi, P. A. (2007) The first shelly fauna from metamorphic rocks of the Sierras Pampeanas (La Cébila Formation, Sierra de Ambato, Argentina): age and paleogeographic implications. *Ameghiniana*, **44** (2), 493–498.

Webring, M. (1985) SAKI: a fortran program for generalized linear inversion of gravity and magnetic profiles. USGS Open File Report, Reston, USA, 85–122.

Whitman, D., Isacks, B.L. & Kay, S.M. (1996) Lithospheric structure and along-strike segmentation of the central Andean Plateau: topography, tectonics, and timing. *Tectonophysics*, **259**, 29–40.

Zhang, C., Mushayandebvu, M.F., Reid, A.B., Fairhead, J.D. & Odegard, M.E. (2000) Euler deconvolution of gravity tensor gradient data. *Geophysics*, **65**, 512–520.

Manuscript received 10 February 2011; In revised form 10 December 2011; Manuscript accepted 15 December 2011.